Observations of the eruption of the Sarychev volcano and simulations using the HadGEM2 climate model.

James M. Haywood, Andy Jones, Lieven Clarisse, Adam Bourassa, John Barnes, Paul Telford, Nicolas Bellouin, Olivier Boucher, Paul Agnew, Cathy Clerbaux, et al.

Observations of the eruption of the Sarychev volcano and simulations using the HadGEM2 climate model

James M. Haywood,[1,2,3] Andy Jones,[2] Lieven Clarisse,[4] Adam Bourassa,[5] John Barnes,[6] Paul Telford,[7] Nicolas Bellouin,[2] Olivier Boucher,[2] Paul Agnew,[8] Cathy Clerbaux,[9] Pierre Coheur,[4] Doug Degenstein,[5] and Peter Braesicke[7]

[1]   In June 2009 the Sarychev volcano located in the Kuril Islands to the northeast of Japan erupted explosively, injecting ash and an estimated 1.2 ± 0.2 Tg of sulfur dioxide into the upper troposphere and lower stratosphere, making it arguably one of the 10 largest stratospheric injections in the last 50 years. During the period immediately after the eruption, we show that the sulfur dioxide (SO_2) cloud was clearly detected by retrievals developed for the Infrared Atmospheric Sounding Interferometer (IASI) satellite instrument and that the resultant stratospheric sulfate aerosol was detected by the Optical Spectrograph and Infrared Imaging System (OSIRIS) limb sounder and CALIPSO lidar. Additional surface-based instrumentation allows assessment of the impact of the eruption on the stratospheric aerosol optical depth. We use a nudged version of the HadGEM2 climate model to investigate how well this state-of-the-science climate model can replicate the distributions of SO_2 and sulfate aerosol. The model simulations and OSIRIS measurements suggest that in the Northern Hemisphere the stratospheric aerosol optical depth was enhanced by around a factor of 3 (0.01 at 550 nm), with resultant impacts upon the radiation budget. The simulations indicate that, in the Northern Hemisphere for July 2009, the magnitude of the mean radiative impact from the volcanic aerosols is more than 60% of the direct radiative forcing of all anthropogenic aerosols put together. While the cooling induced by the eruption will likely not be detectable in the observational record, the combination of modeling and measurements would provide an ideal framework for simulating future larger volcanic eruptions.

1. Introduction

[2]   The explosive eruption of volcanoes is known to exert a significant sporadic effect upon climate. *Robock* [2000] provides a review of the conditions required for a volcanic eruption to exert a significant climatic impact and suggests that the plume must contain a significant amount of sulfur and it must be sufficiently explosive to penetrate into the stratosphere. Various indices have been developed for quantifying the impact of volcanic eruptions such as the Dust Veil Index (DVI) [*Lamb*, 1970] and the Volcanic Explosivity Index (VEI) [*Newhall and Self*, 1982]. According to *Robock* [2000] and *Deshler and Anderson-Sprecher* [2006], the three most significant eruptions since 1960 are: Agung (1963: VEI = 5, DVI = 800), El Chichón (1982: VEI = 5, DVI = 800), and Mount Pinatubo (1991: VEI = 6, DVI = 1000). Each of these volcanic eruptions led to a significantly enhanced stratospheric aerosol optical depth (AOD) [e.g., *Sato et al.*, 1993]. Pinatubo, for example, which erupted in June 1991, has been estimated to have injected up to 20 Tg of SO_2 into the stratosphere [*Bluth et al.*, 1992] which led to a peak increase in the stratospheric AOD at a wavelength of 550 nm (AOD_{550}) of around 0.15–0.20 [*Sato et al.*, 1993; *Ammann et al.*, 2003].

[3]   Besides these three major eruptions, *Deshler and Anderson-Sprecher* [2006, and references therein] document around 30 more minor volcanic eruptions with VEIs of 3 or more in the period 1960–2003 that they consider stratospherically important in terms of SO_2 injection. In the very

[1]Observational Based Research, Met Office, Exeter, UK.
[2]Climate, Chemistry and Ecosystems, Met Office Hadley Centre, Exeter, UK.
[3]College of Engineering, Mathematics, and Physical Sciences, University of Exeter, Exeter, UK.
[4]Spectroscopie de l'Atmosphère, Service de Chimie Quantique et Photophysique, Université Libre de Bruxelles, Brussels, Belgium.
[5]ISAS, University of Saskatchewan, Saskatoon, Saskatchewan, Canada.
[6]Mauna Loa Observatory, NOAA, Hilo, Hawaii, USA.
[7]NCAS Climate, Centre for Atmospheric Science, University of Cambridge, Cambridge, UK.
[8]Forecasting Research and Development, Met Office, Exeter, UK.
[9]UPMC Université Paris 06, Université Versailles St.-Quentin, CNRS/INSU, LATMOS-IPSL, Paris, France.

Figure 1. Image from the International Space Station of early stages of the eruption of the Sarychev volcano on 12 June 2009. Image courtesy of Earth Sciences and Image Analysis Laboratory, NASA Johnson Space Center. (Available at ftp://eol.jsc.nasa.gov/EFS_highres_ISS020_ISS020-E-9048.JPG.)

recent eruption record, Kasatochi in Alaska injected an estimated 1.4–1.6 Tg of SO_2 into the upper troposphere and lower stratosphere (UTLS) on 8 August 2008 [*Carn et al.*, 2009; *Kravitz et al.*, 2010; *Karagulian et al.*, 2010] where it was sampled and tracked by aircraft, surface and satellite remote sensing methods [e.g., *Martinsson et al.*, 2009; *Hoffmann et al.*, 2010; *Bitar et al.*, 2010; *Prata et al.*, 2010; *Bourassa et al.*, 2010] and modeled using coupled ocean-atmosphere climate models [*Kravitz et al.*, 2010].

[4] Over the course of 12–17 June 2009 the Sarychev volcano (located at 48.1°N, 153.2°E) erupted explosively injecting ash and SO_2 into the UTLS. Figure 1 shows a photograph of the eruption taken from an overpass of the International Space Station on 12 June 2009.

[5] We study this eruption using simulations of the volcanic cloud of SO_2 and the resulting sulfate aerosol from the Met Office Hadley Centre HadGEM2 climate model. Section 2 describes HadGEM2 and the sulfur scheme and the experimental design. In section 3 we document retrievals from the Infrared Atmospheric Sounding Interferometer (IASI) to estimate the quantity of SO_2 injected into the UTLS. In section 4 we evaluate the model SO_2 cloud against the IASI observations. In section 5 we use the Optical Spectrograph and Infrared Imaging System (OSIRIS) limb sounder AODs and Cloud-Aerosol Lidar and Infrared Pathfinder Satellite Observation (CALIPSO) lidar data to assess the geographic and vertical distribution of the resultant sulfate aerosol. Section 6 presents the hemispheric *e*-folding times for SO_2 and sulfate aerosol derived from HadGEM2 and from the observations. Section 7 presents data from a lidar situated at Mauna Loa in Hawaii and colocated AOD data from the

Aerosol Robotic Network (AERONET) Sun photometer network [*Holben et al.*, 1998]. We then assess the impacts on local, regional and hemispheric AODs, surface and top of the atmosphere radiation balance and stratospheric heating rates. These are compared to those due to anthropogenic emissions of aerosol [*Bellouin et al.*, 2008b] in section 8 before conclusions are presented in section 9.

2. HadGEM2, the Model Sulfur Cycle, and Nudging Schemes

[6] HadGEM2-A is the atmosphere-only version of the Hadley Centre Global Environment Model version 2 [*Collins et al.*, 2008], where the sea surface temperatures are specified using climatological values. The atmosphere has a horizontal resolution of 1.25° latitude by 1.875° longitude. The model used here has 60 vertical levels with the model top at around 80 km, and is capable of representing stratospheric dynamical features such as the quasi-biennial oscillation (QBO), the western phase of which is important in dispersing stratospheric aerosols poleward [*Stenchikov et al.*, 2004], and the semi annual oscillation. Of the 60 model levels, 32 levels are in the stratosphere and 28 in the troposphere, 12 of which are in the boundary layer.

[7] The HadGEM2 sulfate aerosol scheme is described by *Jones et al.* [2001] and *Bellouin et al.* [2008b] and was originally designed to simulate gas and aqueous phase oxidation of SO_2 in the troposphere. The primary rate-determining step for conversion of SO_2 to sulfate aerosol in the stratosphere is via gaseous reactions with the hydroxyl radical, which is a function of temperature [*Jones et al.*,

2001]. Oxidation of SO_2 leads to the formation of both Aitken and accumulation sulfate aerosol modes with assumed log-normal size distributions with mode radii, r_n, of 0.0065 μm and 0.095 μm and geometric standard deviations, σ, of 1.3 and 1.4, respectively [*Jones et al.*, 2001]. The model accumulation mode size distribution is a reasonable representation of the optically dominant mode of the Pinatubo stratospheric aerosol which has been fitted by r_n of 0.08 μm and 0.11 μm and σ of 1.66 and 1.39 for large and moderate loadings, respectively [*Deshler et al.*, 2003; *Carslaw and Kärcher*, 2006], although *Stothers* [2001] shows significantly different aerosol size distributions from other eruptions. Measurements of stratospheric aerosol suggest two accumulation modes [*Deshler et al.*, 2003], the largest mode probably develops due to the extreme lifetime of stratospheric aerosol leading to growth by particle coagulation and is not modeled in our study: even dedicated complex stratospheric aerosol models fail to adequately capture this feature [*Carslaw and Kärcher*, 2006]. In HadGEM2, intermodal transfer between the Aitken and accumulation modes is parameterized and gravitational sedimentation of sulfate aerosol is included to ensure a realistic stratospheric aerosol lifetime and transport of particles to the troposphere [*Jones et al.*, 2010a]. For high-latitude eruptions, transfer of aerosol to the troposphere occurs primarily through tropopause folds and to a lesser extent through large-scale subsidence over polar regions [e.g., *Oman et al.*, 2005]. Once in the troposphere, particles are removed via wet and dry deposition.

[8] The sulfur scheme was originally designed to investigate tropospheric aerosols where H_2SO_4 is assumed to be fully neutralized by NH_3 and assumed to exist as $(NH_4)_2SO_4$. We remove this assumption so that sulfate is treated as H_2SO_4 throughout. While this could slightly bias tropospheric sulfate AODs, our emphasis in this study is to best represent aerosols in the UTLS. The refractive index and water of hydration is accounted for using the growth factors from *d'Almeida et al.* [1991]. At a wavelength of 0.55μm and relative humidities of 0%, 25%, 50%, and 75%, the optically active accumulation mode aerosol has a single scattering albedo, ω_o, of 1.0, an asymmetry parameter, g, of 0.56, 0.63, 0.68, 0.73, and a specific extinction coefficient, k_e, of 2.3, 4.1, 6.9, and 11.4 m^2 g^{-1} of pure H_2SO_4 aerosol, respectively. The effective radii at these humidities are 0.13, 0.15, 0.18, and 0.21 μm, respectively. *Stothers* [1997, 2001] suggests that the effective radius of stratospheric particles from the eruptions of Ksudach in 1907 and Pinatubo in 1991 grew from around 0.2–0.3 μm to 0.4–0.5 μm over the time scale of around 1 year. *Russell et al.* [1993] derive effective radii of 0.22 ± 0.06 μm for Pinatubo aerosol around 1 month after the eruption, with the lowest values of around 0.016 μm derived if the aerosol is constrained to a monomodal lognormal distribution. While the effective radius of 0.13–0.15 μm for ambient relative humidities of 0–25% is low in comparison to other studies, we believe that the size distribution is reasonable given that we are studying a relatively fresh sulfate cloud. Indeed, we will show that the increase in the AOD at various wavelengths detected at the Mauna Loa observatory is in reasonable agreement with our assumed size distribution. The HadGEM2 standard AOD diagnostics [*Bellouin et al.*, 2008a, 2008b] are modified to give the approximate stratospheric AOD by integrating over the top 40 model levels rather than over the full 60 levels to remove the impacts of emissions of tropospheric aerosols.

[9] In order to produce the meteorological conditions relevant for the period studied we use the technique of nudging and employ the model setup of *Telford et al.* [2009]. This relaxes the model to operational meteorological analysis data from the European Centre for Medium-range Weather Forecasts (ECMWF) using the addition of nonphysical relaxation terms to the model equations of the form

$$\Delta X = F_m(X) + G\Delta t(X_{ana} - X),$$

where X is the variable adjusted, $F_m(X)$ is the model forcing of variable X, X_{ana} is the variable in the analysis data and G is a relaxation parameter [*Telford et al.*, 2008]. The variables that we adjust are potential temperature and zonal and meridional winds.

[10] The choice of relaxation parameter, although arbitrary, is important, as if it is too small nudging is ineffective, yet too large and the model becomes unstable. The value chosen is the "natural" one of 1/6 h^{-1}, the time spacing of the analysis data. This choice is also vindicated by sensitivity studies to changing this value [*Telford et al.*, 2008]. No nudging is applied above model level 50 (~48 km), with a linear increase in G from 0 at level 50 to its full value at level 45 (~38 km), nor below model level 12 (~2.9 km), with a linear increase in G from 0 at level 12 to its full value at level 15 (~4.5 km).

[11] Nudged simulations are performed with and without SO_2 emissions from the Sarychev eruption. The impact upon a model field Y, that evolves from the nudged simulation when aerosol is included, Y_{aer}, and that which evolves from the nudged simulation when aerosol is not included, Y_{no_aer} can be determined from $Y_{no\_aer} - Y_{aer}$. However, because the model is only nudged to the reanalyses data rather than overwritten by them, the meteorological conditions are not precisely identical, especially near the surface where no nudging is applied directly. The stratospheric aerosols will change the solar irradiance and hence the energy budget at the surface thereby changing surface temperatures which feed back onto fields such as relative humidity and hence cloud. While we allow some of the climate response to stratospheric aerosols to develop in the model, it is clear that we only capture a proportion of it because of the use of prescribed SST and nudging in the free troposphere and stratosphere.

3. Description of the IASI Product

[12] IASI is a Sun-synchronous nadir-looking remote sounder onboard the MetOp-A satellite (launched October 2006), which provides global coverage of the thermal outgoing radiation of the Earth in the range 645–2760 cm^{-1} twice a day. The footprint is around 12 km diameter and the swath width is around 2200 km. The interferometer has a high spectral resolution (0.5 cm^{-1}) and low radiometric noise (~0.2 K at 300 K in the atmospheric window). Primarily designed for meteorological applications, its spatial coverage makes the instrument suitable for monitoring a range of atmospheric species [*Clerbaux et al.*, 2009], in particular for detecting and tracking volcanic SO_2 clouds [*Clarisse et al.*, 2008, 2010].
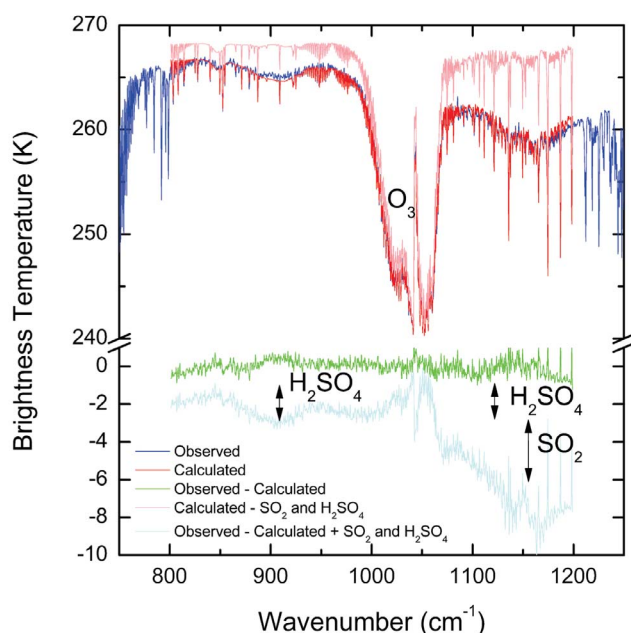
Figure 2. An IASI spectrum (dark blue) observed on 26 June 2010 following the Sarychev eruption. The fitted spectrum is shown in dark red. The residual (green) is the difference between the observed and the calculated spectrum and is the sum of the IASI noise and spectral features not accounted for in the fit. The pink spectrum is what would have been observed if neither SO_2 nor H_2SO_4 aerosols were present. The difference between this spectrum and the observed spectrum (light blue) shows the SO_2 and H_2SO_4 spectral features present in the observed spectrum.

[13] A first, small SO_2 plume from Sarychev was detected by the IASI near real-time SO_2 alert system (see http://cpm-ws4.ulb.ac.be/Alerts/ and *Rix et al.* [2009]) on 11 June 2009, and many more small plumes (totaling less than 0.1 Tg SO_2) followed until 15 June. On 15 June the first large plume was detected suggesting an emission on 15 June of 0.5 Tg SO_2. On 16 June a second large plume was detected suggesting an emission on 16 June of 0.7 Tg SO_2. The potential error estimate is around 15% leading to a total emission of 1.2 ± 0.2 Tg SO_2. Here we summarize the retrieval approach (a detailed discussion can be found in work by *Clarisse et al.* [2008] and *Karagulian et al.* [2010]) and show a rare nadir observation of stratospheric H_2SO_4.

[14] For the retrieval of SO_2 concentrations from the IASI spectra, the strong ν_3 band of SO_2 around 1363 cm^{-1} was used, which is particularly sensitive to stratospheric SO_2. The retrieval scheme employed for this study is based on that proposed by *Clarisse et al.* [2010] which was also applied in a study of the Kasatochi eruption [*Karagulian et al.*, 2010]. The brightness temperature difference between the channels at 1407.25 cm^{-1} and 1408.75 cm^{-1} (baseline) and the channels at 1371.50 cm^{-1} and 1371.75 cm^{-1} (SO_2) is proportional to the total SO_2 column, and is negligibly affected by absorption from other molecules. The relationship is linear for small concentrations, but saturates for high concentrations as the temperature difference is limited by the temperature of the plume. The constants in the exact formula (see *Clarisse et al.* [2008] for details) depend mainly on temperature and

pressure and can be obtained by performing a representative set of optimal estimation retrievals. In this study optimal estimation retrievals were carried out on 100 spectra within the SO_2 cloud from 15 to 20 June 2009 assuming a fixed cloud altitude of 14 ± 0.5 km based on reports of injection heights up to 13.7 km from Tokyo Volcanic Ash Advisory Centre and the Sakhalin Volcanic Eruption Response Team (SVERT) as documented by the Smithsonian Institute/USGS weekly volcanic activity report (http://www.volcano.si.edu).

[15] The sensitive SO_2 channels at 1371.50 cm^{-1} and 1371.75 cm^{-1} are an accurate measure for reasonably low values of the total SO_2 column (below 150–200 Dobson units (DU), where 1 DU refers to a layer of sulphur dioxide that would be 10 μm thick at standard temperature and pressure and 1 DU is equivalent to approximately 0.0285 g SO_2 m^{-2}). At higher concentrations these channels saturate completely leading to an underestimate in concentrations. For this study we have employed a different set of channels for retrievals with estimated loadings above 150 DU. They are: 1407.5 and 1408 cm^{-1} (baseline) and 1384.75 and 1385 cm^{-1} (SO_2). These SO_2 channels are less sensitive to SO_2 (and hence only a good as a measure for high concentrations), but only start to saturate above 1000 DU.

[16] While strong extinction was found due to volcanic ash in the spectra of 15–17 June, this eruption also allowed some rare infrared observations of sulfuric acid aerosols. Due to their relatively small particle size, these aerosols are rarely seen in nadir observations of thermal outgoing radiation. Exceptions include observations of sulfuric acid following the large eruption of Mount Pinatubo [see, e.g., *Echle et al.*, 1998, and references therein] and observational evidence of long-lived sulfuric acid aerosols after the Kasatochi eruption [*Karagulian et al.*, 2010].
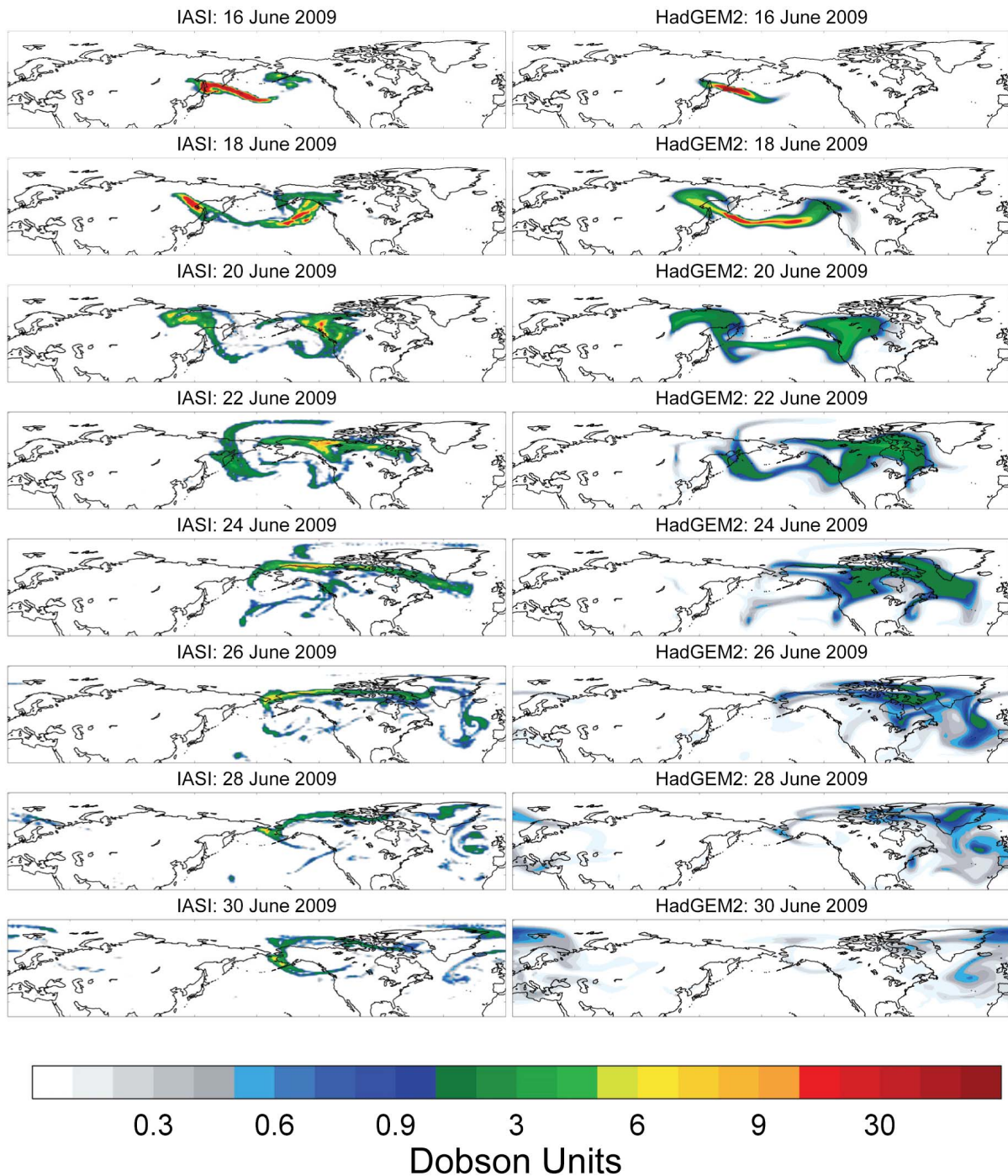
[17] For the Sarychev eruption, strong nadir extinction features of sulfuric acid aerosols were observed around 10 days after the eruption. Figure 2 shows a spectrum observed in the SO_2 cloud on 26 June 2009.

[18] Apart from the usual water vapor lines and ozone absorption feature, the ν_1 band of SO_2 around 1150 cm^{-1} can be observed. Sulfuric acid aerosols have a characteristic wavy extinction feature between 800 and 1200 cm^{-1} (see, e.g., the dip in the spectrum around 900 cm^{-1}), with increasing extinction for increasing wave number (more absorption to the right than to the left of the ozone band).

[19] Figure 2 also shows a calculated spectrum, which was fitted to the observed spectrum using a simultaneous inverse retrieval algorithm of aerosols and molecules [*Clarisse et al.*, 2010]. Sulfuric acid aerosols were modeled in the accumulation mode reported above ($r_n = 0.095$ μm and standard deviation $\sigma = 1.4$).

4. Modeling the Geographic Distribution of the SO_2 Cloud and Validation Using Satellite Data

[20] The simulations of the Sarychev eruption ignore the emissions of 12–14 June (estimated as less than 0.1 Tg) and were initiated for the period 0:00 UTC on 15 June through to 24:00 on 16 June. A total of 1.2 Tg SO_2 was injected into the model UTLS between level 24 and 27 (corresponding to approximately 11 and 15 km) at a constant rate of 0.025 Tg SO_2 hr^{-1}. The injection height is uncertain but was chosen to

IASI: 16 June 2009   HadGEM2: 16 June 2009
IASI: 18 June 2009   HadGEM2: 18 June 2009
IASI: 20 June 2009   HadGEM2: 20 June 2009
IASI: 22 June 2009   HadGEM2: 22 June 2009
IASI: 24 June 2009   HadGEM2: 24 June 2009
IASI: 26 June 2009   HadGEM2: 26 June 2009
IASI: 28 June 2009   HadGEM2: 28 June 2009
IASI: 30 June 2009   HadGEM2: 30 June 2009

0.3   0.6   0.9   3   6   9   30

Dobson Units

Figure 3. The evolution of plumes of SO_2 in Dobson units (DU) for (left) IASI and (right) HadGEM2 for the period 16–30 June 2009.

encompass the reports of injection heights up to 13.7 km (see section 3). Figure 3 shows the evolution of the SO_2 cloud from 16 June through to 30 June 2009, with the left column showing the IASI observations and the right column showing the model simulations.

[21] Figure 3 shows that the position and timing of the SO_2 cloud is relatively well modeled throughout the period. On 16 June there is evidence that the model does not represent the SO_2 cloud to the south of Alaska owing to some ejection of SO_2 into the UTLS before the initial model injection

commenced on 15 June (section 3). As the SO_2 cloud evolves, although the general position is captured, the model results show more evidence of diffusion than the IASI observations. This diffusion reduces numerical instability in relatively coarse resolution models such as HadGEM2 and is an element inherent in semi-Lagrangian and other numerical transport schemes [*Staniforth and Côté*, 1991]. In addition, although the spatial pattern of the SO_2 cloud that is evident in the IASI observations over Alaska during 26–30 June is also evident in the model results, the magnitude is
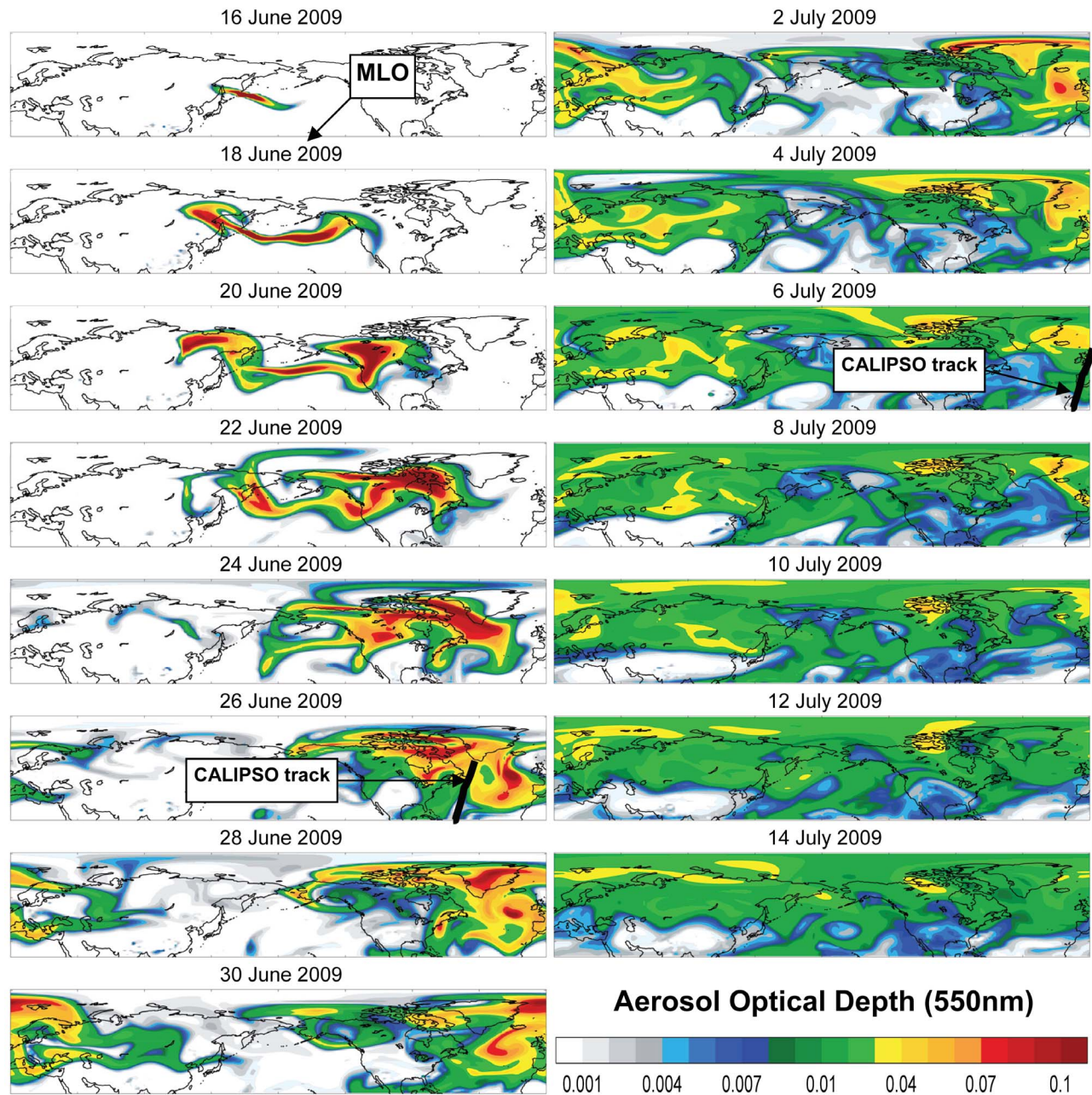
Figure 4. The modeled evolution of sulfate aerosol AOD within HadGEM2 from the Sarychev eruption. The position of the Mauna Loa Observatory (MLO) is marked in the first panel. Selected CALIPSO tracks are also shown for 26 June and 6 July.

underestimated. This may be due to errors in our assumed injection rate or injection altitude, errors in the sulfur scheme, or artifacts from numerical diffusion. The differences between the model and the observations may not all be due to model deficiencies: the practical IASI detection limit appears to be around 0.3–0.5 DU which is why there is generally (but not entirely) a lack of gray colors in the IASI panels shown in Figure 3. It would be possible to iteratively adjust the timing, emission and altitude of the SO_2 injection to more closely match the observed plume [*Prata et al.*, 2007]. However, as the geographic distribution of the SO_2 cloud is reasonably well captured, we retain our simplified emission

rates and injection altitudes. A quantitative comparison of the impact upon the loading of SO_2 in the Northern Hemisphere is presented in section 6.

5. Modeling the Geographic Distribution of the Sulfate Aerosol Cloud and Validation Using Satellite Data

[22] The resulting sulfate aerosol cloud from the oxidation of SO_2 is shown in Figure 4, which shows the AOD at 0.55 μm from 16 June until 14 July 2009.
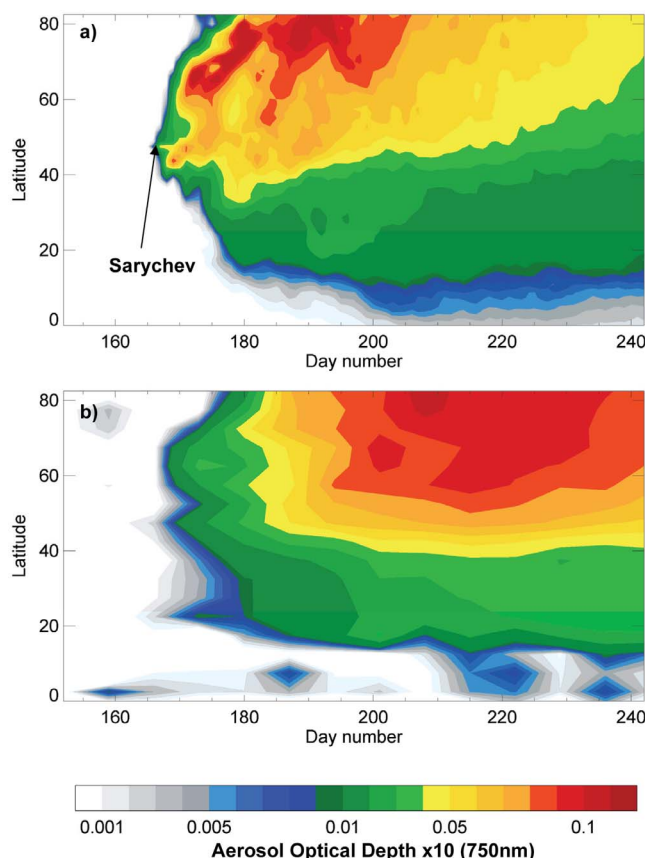
Figure 5. Time versus latitude plots of the aerosol optical depth at 750 nm from (a) HadGEM2 and (b) OSIRIS. The pre-eruption zonal mean AOD is removed from the OSIRIS data to give the perturbation to the AOD.

[23] Figure 4 shows the expected increase in sulfate AOD as the oxidation of SO_2 progresses. By 22 June the modeled sulfate aerosol cloud is centered on North America, by 26 June the aerosol cloud has crossed the Atlantic and is encroaching into Europe, and by 30 June the sulfate cloud has completed one full encirclement of the Earth. Figure 4 also shows the extreme inhomogeneity of the aerosol cloud which is evident throughout the sequence, although the aerosol cloud does become more zonally symmetric as the effects of dilution and dispersion continue. For example, the AOD exceeds 0.1 over significant areas of the North Atlantic during the period 26 June until 2 July while areas of the Pacific have little or no stratospheric AOD. This spatial inhomogeneity is related to the meteorological phenomena that drive the atmospheric circulation. The high AODs over the Atlantic are associated with the development of an upper trough and cutoff surface low-pressure system that persists for several days. Figure 4 suggests that the highest AODs generally occur at latitudes to the north of the eruption, but also that there is significant transport to the south with the entire domain being influenced by the eruption to a greater or lesser extent by 1 month after the eruption.

[24] Validation of the sulfate aerosol cloud is more complex than validation of the SO_2 cloud and is hampered by the relatively small emission (1.2 ± 0.2 Tg SO_2 for Sarychev compared to 20 Tg SO_2 for Pinatubo [Bluth et al., 1992]) and

the lack of readily obtainable data from satellites. Cursory analysis of data from the Moderate Imaging Spectrometer (MODIS) reveals no immediately obvious signal from the sulfate cloud because it overlies tropospheric aerosol which itself displays considerable variability. Data from the Stratospheric Aerosol and Gas Experiment (SAGE), which began providing stratospheric aerosol measurements in 1979, was not available following the early termination of SAGE III in March 2006 due to power failure of the host satellite. However, OSIRIS is currently operational and has been used to monitor the Kasatochi sulfate cloud and validate climate modeling efforts [Kravitz et al., 2010]. We supplement these data with data from the Cloud-Aerosol Lidar and Infrared Pathfinder Satellite Observation instrument (CALIPSO) [Winker et al., 2007].

[25] OSIRIS is a Canadian instrument launched in 2001 on the Swedish Odin satellite [Llewellyn et al., 2004]. OSIRIS measures the vertical profile of limb scattered sunlight spectra and previous work has demonstrated the capability of retrieving information on the vertical distribution of stratospheric aerosol [Bourassa et al., 2007, 2008]. We perform a similar analysis to that of Kravitz et al. [2010] by analyzing the temporal evolution of the zonal mean AOD from OSIRIS which are derived at a wavelength of 750 nm and make a comparison against the AOD derived from the model at the same wavelength. To calculate the perturbation to the AOD from Sarychev from the OSIRIS data, the zonal mean pre-eruption AOD is subtracted from the data. The sampling from OSIRIS will not match the sampling of the model, which could cause some differences between the results, particularly in the early stages after the eruption when the sulfate cloud is inhomogeneous. However, once the sulfate cloud becomes zonally relatively well mixed (which takes around 1 month, Figure 4) the results would be expected to converge.

[26] Figure 5a shows the zonal mean stratospheric sulfate AOD from HadGEM2. The general transport to the north can be seen as the highest AODs are evident north of the eruption latitude as the aerosol is transported in the poleward branch of the Brewer-Dobson circulation, but there is also significant transport to the south in periodic events as also evident in Figure 4. Figure 5b shows the same quantity derived from OSIRIS. The few patches of blue and gray before the eruption and to the south of approximately 10°N are due to the simplistic removal of the pre-eruption stratospheric AOD background and are of no consequence here. Comparison of Figures 5a and 5b shows that the magnitude of the maximum AODs are relatively well produced by the model, as is the north/south gradient. However, the comparison shows that the sulfur scheme in HadGEM2 tends to create high AODs much quicker than observed by OSIRIS, with the maximum occurring at extreme northern latitudes around day 190 (9 July) rather than day 208 (27 July) as suggested by the observations. To further analyze this feature, the temporal evolution of the AOD derived as a function of latitude at 20°N, 40°N, 60°N, and 80°N from the model and as observed by OSIRIS are shown in Figures 6a–6d.

[27] Figure 6 confirms that the magnitude of the maxima in AOD are well represented northward of 40°N, but that they occur much sooner after the eruption in the model than in the observations. At 20°N, the AOD in the OSIRIS observations continues to increase throughout the June–July–August period, while in the model the peak AOD occurs around day
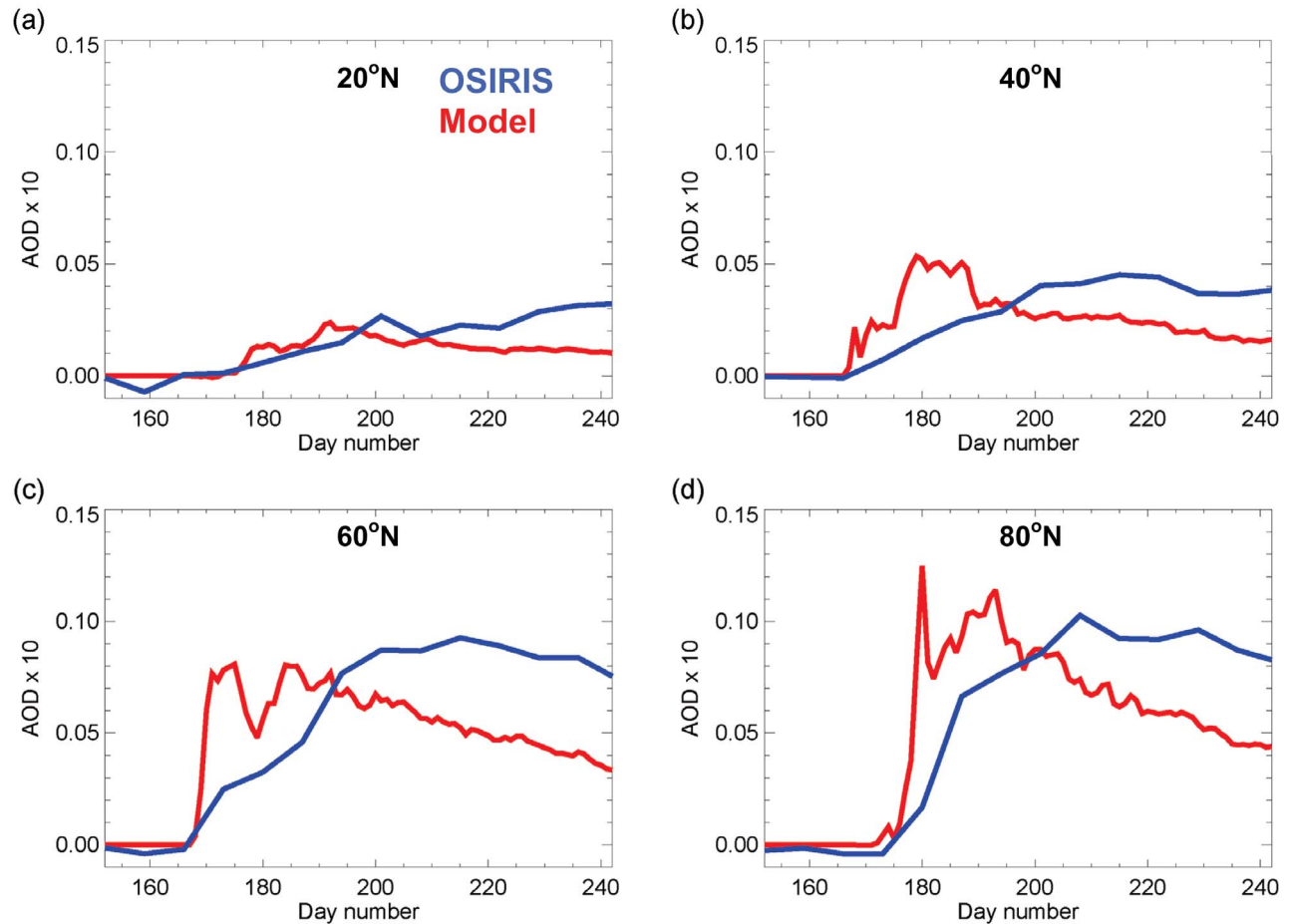
Figure 6. The temporal evolution of the AOD at 750 nm from OSIRIS (blue) and HadGEM2 (red) along four lines of latitude: (a) 20°N, (b) 40°N, (c) 60°N, and (d) 80°N. The pre-eruption zonal mean AOD is removed from the OSIRIS data to give the perturbation to the AOD.

190 (9 July). However, further analysis reveals an *e*-folding time for decrease in $AOD_{0.55}$ of 74 days for HadGEM2 and 75 days for OSIRIS at 60°N, and 60 days for HadGEM2 and 66 days for OSIRIS at 80°N. This suggests that the removal process in terms of the decrease in $AOD_{0.55}$ is relatively well modeled. Further discussion is provided in sections 6 and 9.

[28] The CALIPSO satellite is an integral component of the "A-Train" constellation of satellites and provides unique measurements of aerosol backscatter from space [*Winker et al.*, 2007]. The nature of lidar observations means that the spatial coverage is very limited, but CALIPSO can provide valuable data to confirm the spatial extent and altitude of the sulfate cloud. Graphical data are obtained from browse images (from http://www-calipso.larc.nasa.gov) and show significant stratospheric aerosol in June and July 2009. For brevity we show data from only two overpasses of CALIPSO over the modeled sulfate cloud from 26 June and 6 July 2009. The approximate tracks of CALIPSO over the Atlantic and the western edge of Europe on these days are superimposed on Figure 4 which indicates that aerosol should be readily detectable as these tracks cross areas with large stratospheric AODs.

[29] Figure 7 shows the attenuated backscatter and the modeled aerosol mass mixing ratio for the tracks shown on Figure 4.

[30] A stratospheric aerosol feature is clearly evident (and flagged as such in the data product) at approximately the same altitude and geographic position on both dates. On 26 June, the modeled aerosol layer is in approximately the correct vertical and horizontal position but not as geometrically thin as indicated in the observations; this could be due to the range of altitudes (11–15 km) that were chosen for the injection altitude (section 4) or excessive vertical diffusion in the model. On 7 July the aerosol appears more dilute and diffuse in both the model and the observations, with the aerosol evident in the observations north of 40°N at an altitude of 12–16 km. While the CALIPSO backscatter does not provide direct validation of the aerosol mass mixing ratio, the spatial patterns of the model and observations suggest that the altitude of the injection of the SO_2 and the atmospheric dynamics driving the dispersion of the sulfate cloud are reasonable.

6. Estimation of the Hemispheric *e*-Folding Times of SO_2 and Sulfate Aerosol

[31] The temporal integration of the SO_2 and sulfate clouds over the Northern Hemisphere allows us to estimate and compare the modeled and measured *e*-folding times for SO_2 oxidation to sulfate aerosol and for the removal of sulfate aerosol from the atmosphere.
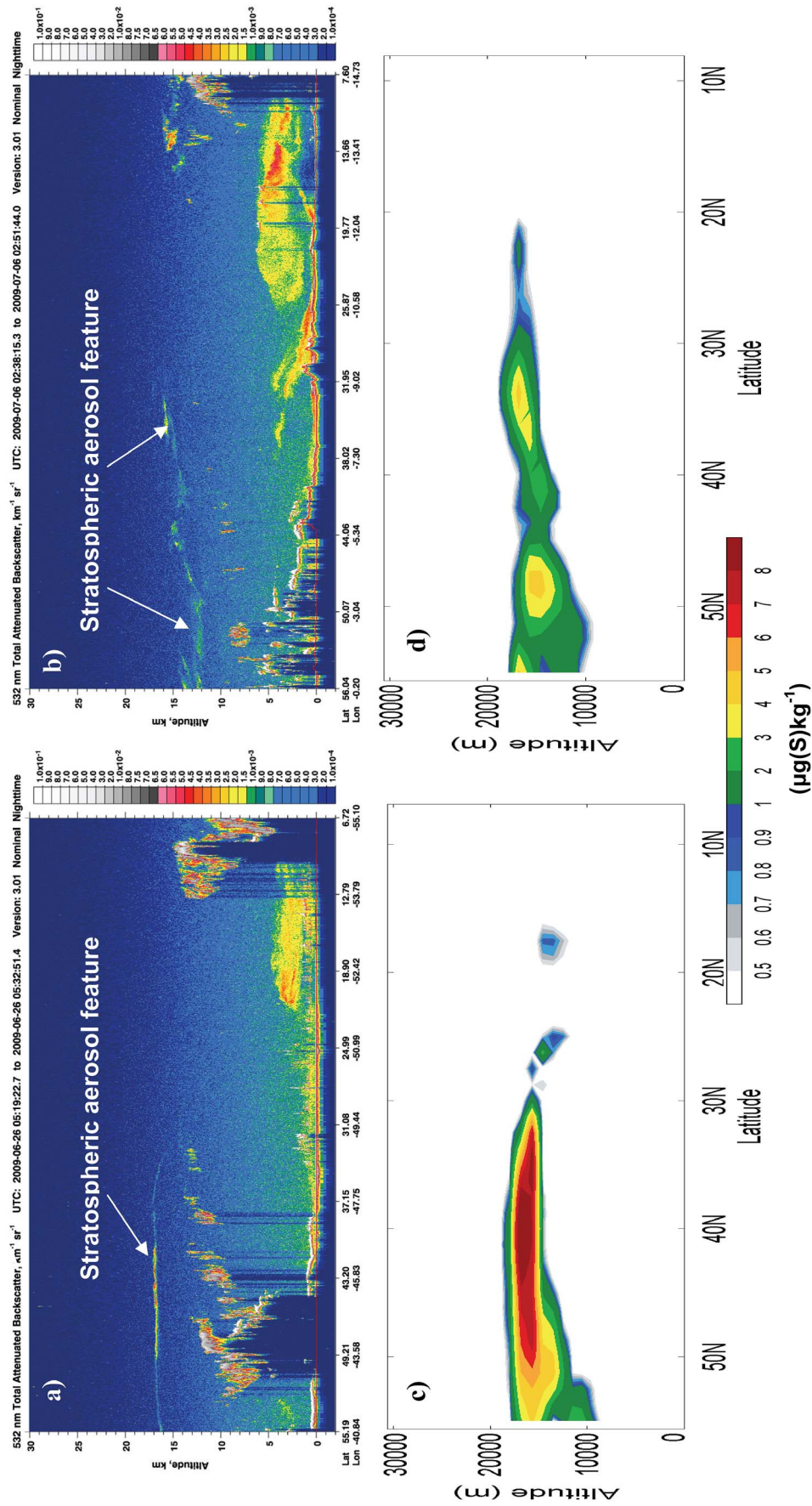
Figure 7. CALIPSO attenuated backscatter (km^{-1} sr^{-1}) for (a) 26 June 2009 and (b) 6 July 2009 for the CALIPSO tracks shown in Figure 4. (c and d) Corresponding simulations of the aerosol accumulation modes mass mixing ratio (μg(S)kg^{-1}). The stratospheric aerosol features identified in the CALIPSO retrievals are highlighted.
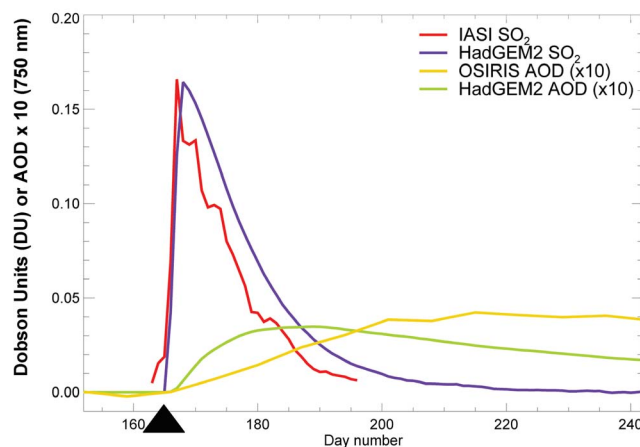
Figure 8. The time evolution of SO_2 derived from IASI (red line) and the model (purple line) averaged over the Northern Hemisphere measured in DU. The modeled sulphate AOD is also shown at 750 nm (green line). The OSIRIS AOD is shown by the yellow line. The approximate time period for the Sarychev eruption is shown by the solid black triangle.

[32] Figure 8 shows that the peak burden estimated from IASI is well modeled; this is no surprise as it is related to the chosen total emission over the period of 1.2 Tg SO_2. The e-folding times over the Northern Hemisphere are 10–11 days for the IASI measurements and 13–14 days for HadGEM2 which on the face of it suggests a ~25% slower oxidation of SO_2 in model. However, there is a complicating factor in that the practical detection limit of IASI of 0.3–0.5 DU (section 4) means that as the plume becomes more diffuse, fewer and fewer pixels exceed the detection limit and consequently the e-folding time determined from IASI will be somewhat quicker than in reality. This effect can be investigated using our HadGEM2 simulations. These suggest a reduction in the e-folding time to around 6–7 days if a detection limit of 0.3 DU is applied to the model fields, a reduction by around 50%. Application of such a correction to IASI would increase the IASI e-folding time to around 20–22 days. However, the HadGEM2 model results are likely to be too dispersive, so a correction to IASI based on the HadGEM2 results will lead to too long an e-folding time. Given these uncertainties and the simplicity of our approach to the emission rate and injection height, the agreement between model and observations is deemed reasonable.

[33] Figure 8 also shows how the HadGEM2 mean Northern Hemisphere AOD evolves. The peak in sulfate AOD_{750} (corresponding to the OSIRIS detection wavelength) is approximately 0.0037 around 25 days after the volcanic plume is initiated indicating that peak modeled hemispheric mean AOD occurs around 1–5 July. The conversion from 750 nm to 550 nm leads to an AOD_{550} of 0.0086. For OSIRIS the peak mean Northern Hemisphere AOD_{750} is around 0.0042, which corresponds to an AOD_{550} of 0.0097.

[34] Subsequently the AOD decreases owing to transfer from the stratosphere to the troposphere by sedimentation and tropopause folding. The modeled hemispheric e-folding time for the removal of sulfate aerosol from the atmosphere (calculated via the impact on AOD) is calculated as being around 71 days. The corresponding hemispheric e-folding

time may also be derived from OSIRIS and is approximately 81 days, which suggests that the removal processes included in the model are reasonably well parameterized. However, the model forms optically active accumulation mode sulfate aerosol (peak AOD 1–5 July) around 1 month quicker than observed by OSIRIS (peak AOD 30 July to 5 August). The reasons for this discrepancy are discussed in section 9.

7. Modeling and Analysis of the Sulfate Cloud Using Surface-Based Data

[35] The Mauna Loa Observatory (MLO, latitude 19.5°N, 155.5°W) is a unique location for monitoring stratospheric events because of its location away from the majority of local pollution sources, but more importantly because at 3400 m the observatory is above the majority of tropospheric aerosols, allowing the stratosphere to be probed by remote sensing measurements such as lidars and Sun photometers with minimal influence from tropospheric constituents. The stratospheric aerosol layer has been monitored with lidars at the MLO since 1975 allowing monitoring of volcanic eruptions [e.g., *Barnes and Hofmann*, 1997] and stratospheric aerosol trends. These trends may be related to increases in tropospheric emissions of SO_2 in Asia where convective activity can penetrate the stratosphere, thereby increasing stratospheric burdens [e.g., *Hofmann et al.*, 2009]. The current MLO lidar is an Nd:YAG lidar (532 and 1064 nm wavelength) which began operation in 1994 and measurements are typically performed once a week. The analysis presented here is the integrated backscatter (neglecting attenuation) at altitudes of 15–20 km; below this altitude the presence of cirrus clouds can contaminate results. The measurement sequence of most interest to the analysis presented here is from measurements on 1, 8, and 15 July 2009 (day 182, 189, and 196). Data from 22 July (day 203) is missing owing to potential contamination by cirrus cloud, but the measurements are available from 29 July (day 210) onward. Figure 9 shows the backscatter integrated over the range 15–20 km (sr^{-1}) for the whole of 2008 and 2009.

[36] Figure 9 shows a marked increase in the integrated backscatter (IB) on day 182 (1 July) in 2009 followed by a return to unperturbed values before increasing on day 196 (15 July) 2009 and remaining elevated when compared with 2008. Note that the MLO lidar also shows a step increase in the IB on day 260 (17 September) of 2008 which appears to be associated with the eruption of Kasatochi on 7 August 2008 [*Carn et al.*, 2009]. In the absence of significant volcanic stratospheric aerosol, it appears that the background IB level in the summer would be approximately 0.00005 sr^{-1}. The eruption of Sarychev has therefore raised the IB by about 0.00008 to 0.00013 sr^{-1}. Making the simple assumption that the IB is proportional to the AOD (i.e., assuming that the aerosol size distribution and scattering properties do not change significantly between pre-eruption and posteruption) suggests an increase in the AOD between 15 and 20 km of a factor of 2.6. If we assume that the 532 nm extinction to backscatter ratio is approximately 50 ± 25 [*Jäger and Deshler*, 2002, 2003; *Thomason et al.*, 2007] then an increase in the AOD of around 0.004 ± 0.002 is approximated over the layer 15–20 km.

[37] Level 2.0 AERONET data [*Holben et al.*, 1998] is also available from Mauna Loa. Although AERONET data
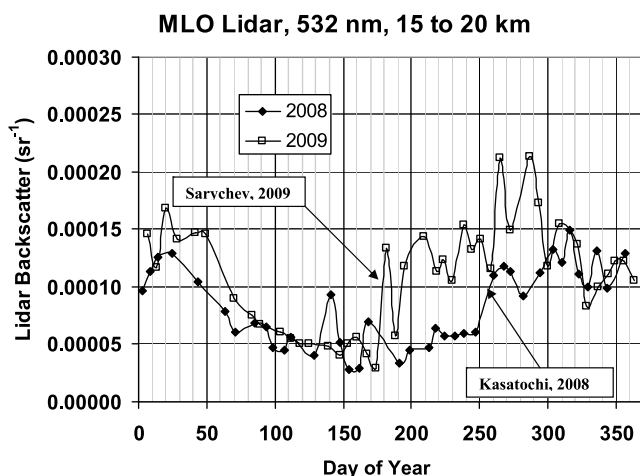
Figure 9. The evolution of the NOAA/ESRL Mauna Loa Observatory (MLO) lidar backscatter at 532 nm integrated between 15 and 20 km for the years 2008 and 2009.

determines the total column AOD at a number of wavelengths, the altitude of the station (3400 m) mean that the majority of tropospheric aerosols and their high temporal variability are excluded from the measurements. Sun photometer observations from Mauna Loa have previously been used in investigating the impacts of Pinatubo [e.g., *Russell et al.*, 1993]. We restrict our analyses to July and August 2009: before this period no statistically significant differences are evident and after this period the Kasatochi eruption of 2008 may influence the mean AODs derived over the period 1996–2008 (Figure 9).

[38] During July and August 2009 five out of six of the measured (rather than interpolated) wavelength-dependent AODs are significantly higher (at the 95% significance level) than the mean determined from the period 1996–2008 (Table 1). Even the 675 nm AOD in 2009 is on the margin of being significantly higher than the mean.

[39] The wavelength dependence of the aerosol specific extinction or of AOD, which is frequently characterized by the Ångström exponent, Å, is defined by

$$\text{Å} = -\ln(AOD_1/AOD_2)/(\lambda_1/\lambda_2),$$

where λ is the wavelength. The increase in the AOD over the 2 months from AERONET suggests an $\text{Å}_{(440/675)}$ of 1.4 for July and 2.4 for August. The higher value of $\text{Å}_{(440/675)}$ in August rather than July is counterintuitive as it suggests more small particle influence during August than July. However, during July, the site is unlikely to be influenced by stratospheric aerosol all of the time (see, e.g., Figure 4), which may explain this discrepancy, particularly if we consider that the model appears to produce optically active sulfate aerosol rather too quickly (sections 6 and 9). However, such high values of $\text{Å}_{(440/675)}$ are associated with small particles. Our assumed lognormal size distribution with a $r_n = 0.095$ and a $\sigma = 1.4$ predicts $\text{Å}_{(440/675)}$ of 2.6–2.4 for low relative humidities of 0–25% typical of the stratosphere, which are in good agreement with the observed $\text{Å}_{(440/675)}$ for August. If we were to use the observed bimodal distribution for $\text{Å}_{(440/675)}$ discussed in section 2 [*Deshler et al.*, 2003;

Carslaw and Kärcher, 2006] for moderate stratospheric loadings, $\text{Å}_{(440/675)}$ is 0.7–0.5 which does not agree well with the observed $\text{Å}_{(440/675)}$ for August. While we acknowledge that our analysis of AERONET could be enhanced by analysis of the spectral radiances and subsequent inversions to determine the best aerosol size distribution [e.g., *Dubovik et al.*, 2002], such research is beyond the scope of the current paper.

[40] The discrepancy between the increase in the AOD over July–August between the lidar (0.004 ± 0.002 at 532 nm) and AERONET (a mean of 0.009 ± 0.004 at 532 nm) may be due to a combination of factors. The lidar may not capture the vertical extent of the volcanic cloud because the integrated backscatter is calculated over the range 15–20 km. The lower level is chosen to remove the impacts of any cirrus from the retrievals, but there could be significant aerosol loading below this level, leading to an underestimation of the AOD. Second, the assumed backscatter ratio of 50 could be significantly in error for the relatively fresh aerosol cloud from Sarychev. Similarly, there could be significant errors from our analysis of AERONET which measures the AOD through the entire column of the atmosphere, and will be influenced by interannual variability in upper tropospheric aerosols. Nevertheless, both methods suggest that there is a significant detectable perturbation to the stratospheric AOD caused by the Sarychev eruption.

[41] Figure 10 shows the corresponding analysis of the change in the stratospheric AOD diagnosed in HadGEM2 over Mauna Loa.

[42] The model shows a weak increase in the stratospheric AOD from around day 180 (29 June), although the major influence of the stratospheric sulfate cloud only exceeds 0.004 subsequent to day 188 (7 July) (see also Figure 4). The mean modeled increase in the stratospheric AOD at 550 nm for July and August is approximately 0.0038. Thus, while the exact details of the MLO observations are not well represented in terms of the timing or the variability, the general influence of the Sarychev sulfate cloud commencing from the beginning of July lies close to that derived from the MLO lidar.

[43] Further analysis has been performed using the two multiwavelength Raman lidars located at Potenza, Italy, by

Table 1. AOD at 440, 500, and 675 nm for July and August 2009 and the Mean Obtained From the Period 1996–2008[a]

Wavelength (nm)	2009	Mean 1996–2008 Level 2.0 Data	2009–Mean
		July	
440	0.028	0.015 ± 0.006	+0.013
500	0.022	0.011 ± 0.005	+0.011
532	*0.020*	*0.010 ± 0.004*	*+0.010*
550	*0.019*	*0.010 ± 0.004*	*+0.009*
675	0.013	0.006 ± 0.004	+0.007
		August	
440	0.024	0.013 ± 0.006	+0.011
500	0.018	0.010 ± 0.004	+0.008
532	*0.016*	*0.008 ± 0.004*	*+0.008*
550	*0.015*	*0.008 ± 0.004*	*+0.007*
675	0.009	0.005 ± 0.004	+0.004

[a]The values at 532 and 550 nm shown in italics are derived by interpolation from the measured Ångström exponent. The ± figures represent twice the standard deviation (the 95% significance level). The difference between the 2009 values and the means is also shown.
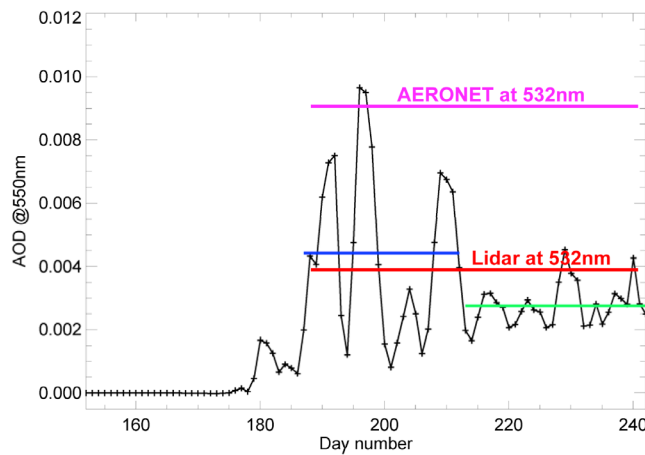
Figure 10. The evolution of the modeled stratospheric aerosol optical depth over Mauna Loa at 550 nm. The blue and green lines show the average AOD during July and August 2009, respectively, and the red and purple lines show those derived from the lidar and from AERONET for the July–August period.

d'Amico et al. [2010] who conclude that the timing of the arrival of the sulfate cloud over the site is well modeled by the HadGEM2 simulations. Furthermore, *d'Amico et al.* [2010] are able to assess the AOD$_{355}$ for 12 and 31 August 2009, deriving AODs of 0.018 and 0.014 from their lidar techniques; the corresponding AOD$_{355}$ predicted by the model are 0.015 and 0.011 respectively. Given a background stratospheric AOD of around 0.002 that is not simulated in the model, the results are in remarkable (and perhaps fortuitous) agreement.

8. Analysis of the Impact Upon Meteorological Variables

[44] As pointed out by *Kravitz et al.* [2010], volcanic eruptions of the magnitude and at the latitude of Sarychev have negligible impact upon climate. We compared two 10 member ensembles using a free-running version of the HadGEM2-A model and were unable to detect statistically significant differences in the major meteorological variables owing to the natural weather variability. However, the impact on certain meteorological variables can be assessed using the nudged model simulations. Variables such as the impact upon the solar radiation budget at the surface and at the top of the atmosphere (TOA) and the approximate radiative forcing exerted by the volcanic aerosol can be estimated. The impact upon these parameters can be approximated from the difference between a model field Y, that evolves from the nudged simulation when aerosol is included, Y_{aer}, and that that evolves from the nudged simulation when aerosol is not included, Y_{no_aer}. Although the model evolution is nudged to evolve to resemble the ECMWF analyses (section 2), the exact evolution of the two model runs does differ slightly leading to some differences in, e.g., the cloud fields. This can lead to some noise in the resultant $Y_{no\_aer} - Y_{aer}$ fields, but does not significantly affect the results, except where explicitly noted in the analyses that follow.

[45] The left column of Figure 11 shows the evolution of the TOA clear sky shortwave radiative impact (technically the direct clear sky shortwave radiative impact, but we drop the word direct to avoid confusion with the impact on direct and diffuse radiation) determined from $SW_{cs\_TOA\_no\_aer} - SW_{cs\_TOA\_aer}$ where $SW_{cs\_TOA\_aer}$ and $SW_{cs\_TOA\_no\_aer}$ correspond to the TOA upwelling shortwave radiation with and without aerosols, respectively. The change in the surface solar irradiance is spatially very similar and is not shown for brevity, but is larger in magnitude by around 10% owing to the increase in the effective path length of scattered radiation allowing more gaseous absorption.

[46] Not surprisingly, the impact on solar irradiances follows the stratospheric sulfate AOD patterns. The magnitude of the impact in clear skies is in the range -4 to -6 W m^{-2} over significant parts of the north Atlantic during the period 24 June to 2 July 2009. As the values represent diurnal averages, the local daytime impact on the solar radiation at the surface will reach -10 W m^{-2} in these areas. However, at this magnitude, it is difficult to definitively separate the impact of stratospheric aerosols from the impacts of tropospheric aerosols and the impacts of thin cirrus clouds on observations of the solar irradiance at the surface.

[47] The all-sky radiative impact cannot be clearly determined from $SW_{TOA\_no\_aer} - SW_{TOA\_aer}$ because of the slight differences in the evolution of cloud in the models, so an alternative approach is used. For a purely scattering aerosol, the all-sky shortwave radiative impact may be approximated by multiplying the clear-sky TOA radiative effect at each time step by $(1-A_c)$ where A_c is the cloud fraction [*Haywood et al.*, 1997]. This method essentially assumes that the contribution to the radiative impact from cloudy areas is negligible, which radiative transfer calculations have shown to be a reasonable assumption for conservative scattering from sulfate aerosol particles [*Haywood and Shine*, 1997] for optically thick cloud. The right column of Figure 11 shows the evolution of the all-sky TOA radiative impact calculated in this manner, which differs considerably from the pattern of the clear sky impact shown in the left column owing to cloud masking procedure.

[48] To determine the significance of the perturbation to the climate system we compare the perturbations in the modeled stratospheric AOD from the Sarychev eruption for July 2009 with that due to anthropogenic sulfate, nitrate, biomass burning, black carbon, and fossil fuel soot aerosols. *Bellouin et al.* [2008a] show that simulations of AOD from HadGEM2 are in reasonable agreement with those from satellite observations. Furthermore, the annual mean direct radiative forcing determined from HadGEM2 (-0.16 W m^{-2}) is in reasonable agreement with the results from AeroCom (-0.2 W m^{-2} with standard deviation 0.2 W m^{-2}) [*Schulz et al.*, 2006]. These two facts suggest that the radiative forcing derived from HadGEM2 is reasonably representative of typical model simulations. The global distribution of AOD at 550 nm of tropospheric anthropogenic aerosol is shown in Figure 12a, while those showing the modeled volcanic stratospheric aerosol are shown in Figure 12b.

[49] Figures 12a and 12b show that in remote regions of the Northern Hemisphere, the AOD from Sarychev can be of comparable magnitude or even dominate the AOD from anthropogenic emissions. The ratio of the AOD at 550 nm
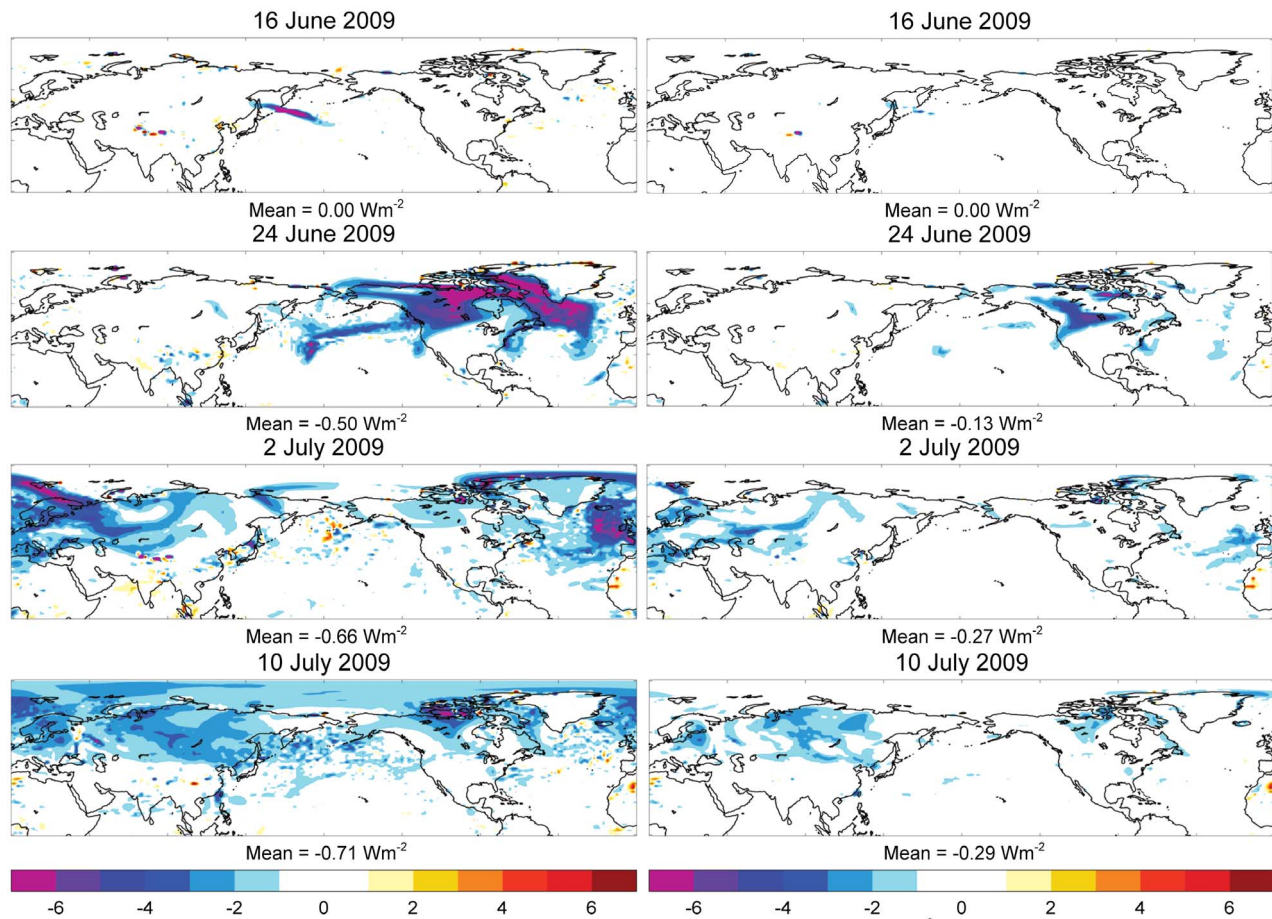
Figure 11. The change in the Northern Hemisphere irradiances (W m^{-2}): (left) clear-sky TOA net short-wave impact; (right) all-sky TOA radiative impact.

from Sarychev to that from anthropogenic emissions is around 10% for the Northern Hemisphere.

[50] Figure 12c shows the direct radiative forcing from anthropogenic aerosols calculated as the difference between the year 2000 and preindustrial times estimated in HadGEM2 using AeroCom emissions. Figure 12d shows the radiative impact from Sarychev. In the Northern Hemisphere, the radiative impact of the Sarychev volcano is some 63% of that caused by all anthropogenic emissions of aerosol put together. The reason that the radiative impact of Sarychev is 63% of the direct anthropogenic impact, while the AOD is only 10%, is that the anthropogenic aerosol is more absorbing and therefore less efficient at exerting a negative radiative forcing at the TOA [*Haywood and Shine*, 1995].

[51] The final meteorological variable that is modeled is the impact on the zonal mean near surface land temperature as shown in Figure 13. Note that, in these simulations, the response in near-surface temperature is only diagnosed over land areas because prescribed climatological sea surface temperatures are used that inhibit near-surface temperature changes over ocean regions. Note also that the use of the nudged model means that large-scale dynamical feedbacks are inhibited. This has the advantage of significantly reducing the weather variability so that a signal can be detected without running a large number of ensemble members [see, e.g., *Kravitz et al.*, 2010]. Thus the temperature response that is

shown here may be considered to be an approximate and incomplete response to the change in the surface radiative fluxes noted above.

[52] The zonal mean temperature change for both July and August shows some significant noise, but a similar pattern for both months; the cooling is strongest (−0.05 K) at higher latitudes and reduces to close to zero by around 30°N. These results suggest that even if a volcanic eruption of the magnitude of Pinatubo (20 Tg SO_2) were to occur at high latitudes, the induced zonal mean radiatively driven cooling at the surface would be less than 1 K for the months following the eruption, which would be difficult to detect given the much higher variability in near surface temperatures at high latitudes. Thus, as concluded by *Oman et al.* [2005] and *Kravitz et al.* [2010], the climatic impacts from high-latitude eruptions are very much reduced when compared to tropical eruptions.

9. Discussion and Conclusions

[53] This study provides a first analysis of the eruption of Sarychev in the Kuril Islands to the northeast of Japan in June 2009. The use of an atmospheric general circulation model nudged to ECMWF operational analysis data allows the transport of the SO_2 cloud, the associated sulfate aerosol and the radiative impacts to be validated against dedicated
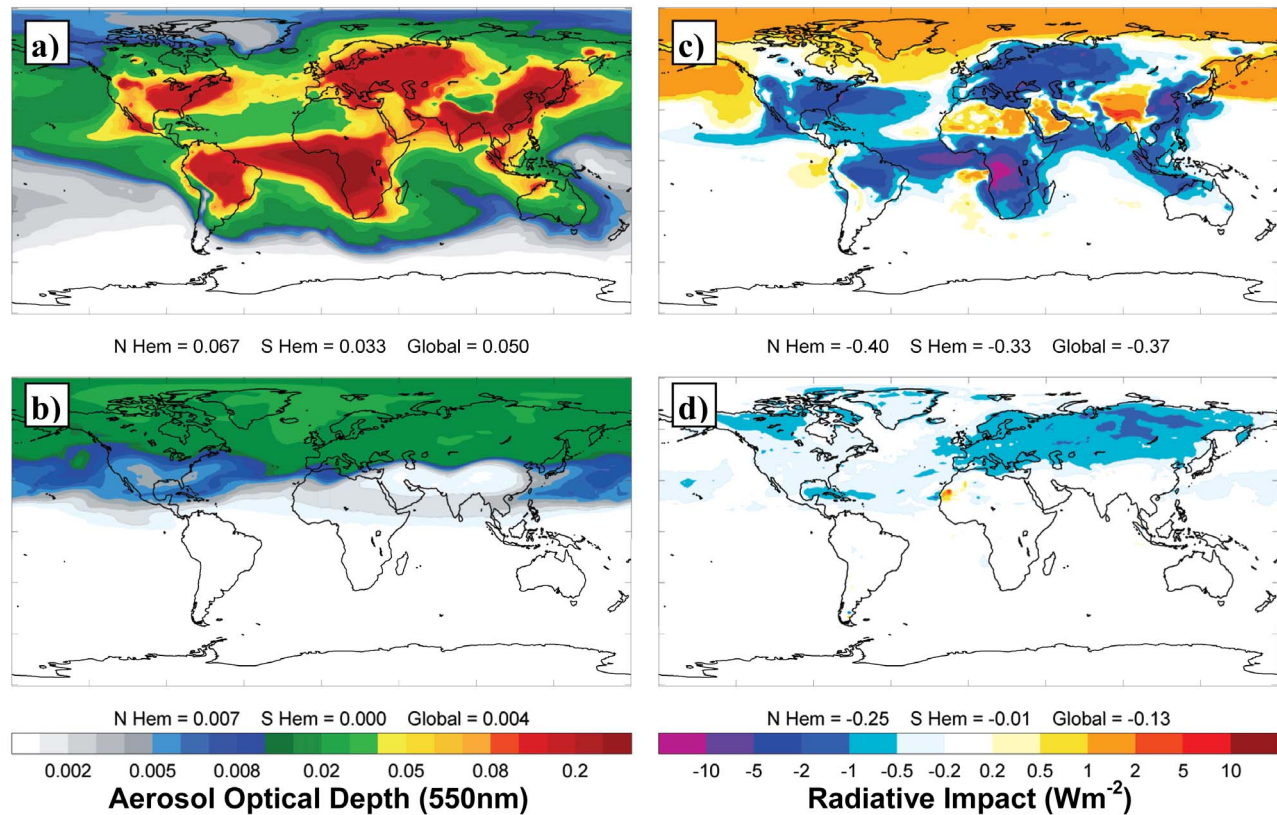
Figure 12. The aerosol optical depth for July at 550 nm derived for (a) anthropogenic aerosol and (b) the Sarychev stratospheric aerosol plume. The radiative forcing or radiative impact (W m^{-2}) for (c) anthropogenic aerosol and (d) the Sarychev stratospheric aerosol plume. The radiative forcing for anthropogenic aerosol is calculated as the difference between anthropogenic and natural aerosols for the year 2000 and those for the year 1860.

retrieval algorithms. An enhanced retrieval algorithm is described for detecting the SO_2 cloud allowing an estimate of the total injection of $\sim 1.2 \pm 0.2$ Tg SO_2 making it arguably one of the 10 largest stratospheric injections in the last 50 years. Table 2 shows an approximate ranking in terms of the injection of sulfur dioxide into the stratosphere and the perturbation to the stratospheric aerosol AOD at 550 nm, although there are some considerable uncertainties in deriving such a ranking owing to the lack of satellite observations of SO_2 before around 1980.

[54] The retrieval algorithm allows a detailed geographic mapping of the evolution of the SO_2 cloud. The IASI retrieval indicates that the Sarychev SO_2 cloud sequentially crossed the North Pacific, North America, and the North Atlantic in a period of around 10 days. HadGEM2, when nudged to ECMWF operational analysis data, is able to represent the main features of the dynamical evolution of the SO_2 cloud with reasonable consistency. The e-folding times for the oxidation of SO_2, determined over the Northern Hemisphere for the period 16 June to 1 July, are 10–11 days for the IASI measurements and 13–14 days for HadGEM2, which suggests a $\sim 25\%$ slower oxidation of SO_2 in the model. While care must be taken in accounting for the detection limit thresholds in the IASI retrievals, which will lead to too fast an e-folding time, these results appear very different to those observed and modeled for the oxidation of SO_2 after

the Pinatubo eruption where the e-folding time was estimated as being between 30 and 40 days [e.g., *Bluth et al.*, 1997, and references therein] presumably because of differences in the injection altitude and latitude.

[55] In terms of stratospheric aerosol, the model suggests that the sulfate aerosol encircles the Earth in around 14 days. While SO_2 detection has been possible using the Ozone Monitoring Instrument (OMI) [e.g., *Krotkov et al.*, 2006; *Prata et al.*, 2007; *Yang et al.*, 2007] and IASI [*Clarisse et al.*, 2008, 2010] detection of stratospheric aerosols from low VEI eruptions is more challenging to detect from space owing to the low stratospheric loading. However, *Thomason et al.* [2007] demonstrate that stratospheric aerosol was detected subsequent to the minor eruptions of Soufriere Hills volcano (Montserrat, May 2006) and Rabaul (October 2006). In our study, we demonstrate that the stratospheric perturbation from the Sarychev eruption is sufficient for detection with the OSIRIS limb sounder and the CALIPSO lidar. The geographic pattern detected by OSIRIS shows many similarities to that reported by *Kravitz et al.* [2010] for the Kasatochi eruption, which is not surprising as the time of year, altitude of injection and eruption latitude of Kasatochi (August 2008, 10–16 km, 48°N) were similar to that of Sarychev (June 2009, 11–15 km, 52°N). The Northern Hemisphere maximum perturbation in AOD_{550} for the Sarychev eruption derived from both the model and the OSIRIS measurements is 0.0087
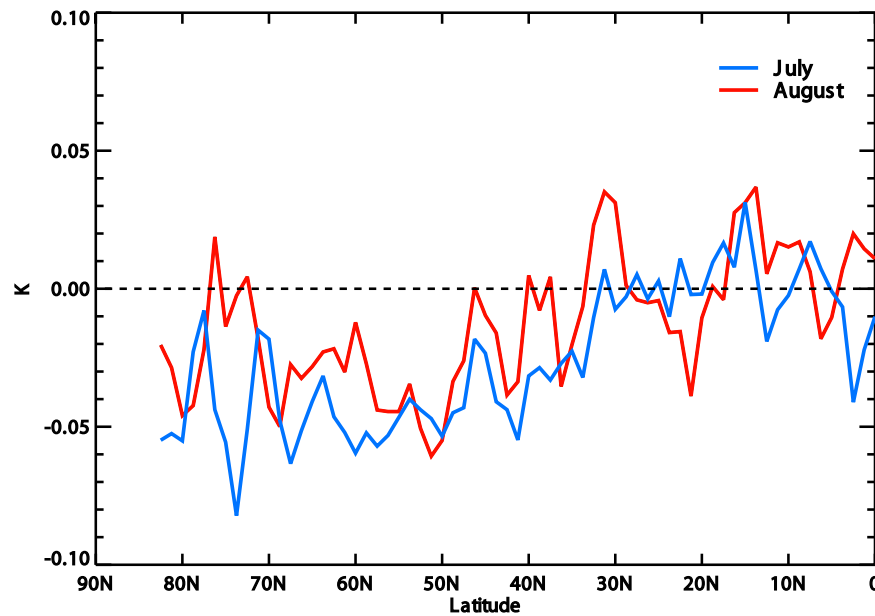
Figure 13. The radiatively driven change in the near-surface temperature over land as a function of latitude for July and August 2009 calculated by HadGEM2.

and 0.0098, respectively, suggesting a maximum global mean perturbation to the stratospheric AOD_{550} of around 0.005. Kasatochi/Okmok were estimated to inject 1.4–1.6 Tg SO_2 [*Carn et al.*, 2009; *Kravitz et al.*, 2010] into the UTLS. We use OSIRIS data from 2008 and identical methodology to that for our Sarychev results and determine the maximum Northern Hemisphere mean AOD at 750 nm for Kasatochi of around 0.002 which translates to a global mean AOD_{550} perturbation of 0.0023. Although not investigated fully here, it appears that the perturbation to the stratospheric AOD_{550} is larger for Sarychev than for the Kasatochi/Okmok eruptions.

[56] *Kravitz et al.* [2010] determined that the GISS ModelE simulations produced AODs from the Kasatochi eruption that were, on the face of it, 1 order of magnitude higher than OSIRIS. *Kravitz et al.* [2010] report that even if AOD wavelength corrections and factors to account for missing AOD from the lowermost part of the limb sounding in OSIRIS are accounted for, ModelE remains at best a factor of 2 to 3 higher than the OSIRIS observations. Our simulations show much better agreement in the peak AODs in terms

of global, hemispheric and zonal means. As pointed out by *Kravitz et al.* [2010], a significant source of uncertainty in deriving the AOD at 750 nm comes from the assumed size distribution. *Kravitz et al.* [2010] assume a size distribution with a dry effective radius of 0.25μm, which is approximately twice as large as that used in our modeling study, and determine that the ratio of $AOD_{750}/AOD_{550} = 0.8$. We believe that our assumed size distribution, with smaller geometric mean radius, is more representative of fresh aerosol. Our size distribution yields $AOD_{750}/AOD_{550} = 0.43$ and thus could improve the agreement between OSIRIS and ModelE simulations for the Kasatochi eruption. However, we agree with *Kravitz et al.* [2010] that the paucity of validation data seriously hampers comprehensive model validation efforts.

[57] We determine a hemispheric *e*-folding time for removal of sulfate aerosol of around 71 days from HadGEM2, and 81 days from OSIRIS. These *e*-folding times are significantly shorter (~15%) than that of 12–14 months estimated for the Pinatubo eruption [*Baran and Foot*, 1994; *Barnes and Hofmann*, 1997]. This is because the Sarychev

Table 2. Ranking of the Impact of Volcanoes Upon the Stratospheric Aerosol Optical Depth (550 nm)

Ranking	Volcano	Eruption Date	SO_2 Injection (Tg)	Change in AOD at 550 nm
1	Pinatubo	June 1991	20[a]	0.15[b]–0.20[c]
2	El Chichón	March–April 1982	7–12[a]	0.10[b]–0.14[c]
3	Agung	March–May 1963	not available	0.09[b]–0.14[c]
4	Fernandina	June 1968	not available	0.033[b]–0.05[c]
5	Fuego	October 1974	not available	0.03[b]–0.04[c]
6	Awu	August 1966	not available	0.02[b]
7	Cerro Hudson	August 1991	1.5[a]	0.009[b]
8	Nevado del Ruiz	November 1985	0.7[a]	0.006[b]
9	Sarychev	June 2009	1.2[d]	0.005[d]
10	Kasatochi	August 2008	1.4–1.6[e]	0.0023[d]

[a]*Bluth et al.* [1992, and references therein].
[b]*Sato et al.* [1993].
[c]*Ammann et al.* [2003].
[d]This study.
[e]*Carn et al.* [2009].

SO$_2$ injection was at lower altitude and higher latitude than Pinatubo, and the aerosol is therefore subject to more rapid transfer to the troposphere via sedimentation, tropopause folding, and large-scale subsidence over polar regions [e.g., *Oman et al.*, 2005] where it is removed by wet deposition.

[58] While the *e*-folding times for the conversion of SO$_2$ to H$_2$SO$_4$ and the removal of H$_2$SO$_4$ appear relatively well modeled, the peak AODs in the OSIRIS data are observed approximately 1 month later than in HadGEM2. This leads us to conclude that the rate of transfer from optically inactive Aitken to optically active accumulation mode aerosol is too fast in the model. Indeed, the CLASSIC aerosol scheme used in HadGEM2 [*Bellouin et al.*, 2008b] does not explicitly represent nucleation of new aerosol particles which is the first step in sulfate aerosol formation in the stratosphere. In the troposphere, the neglect of the nucleation of new particles can lead to insufficient aerosol dispersion and low AODs far from sources. This problem will likely be exacerbated in the stratosphere, where gas phase reactions rather than aqueous phase reactions dominate. Such a deficiency has been noted in the CLASSIC aerosol scheme and is currently being addressed in the UK Chemistry and Aerosol (UKCA) scheme which explicitly includes aerosol nucleation [*Johnson et al.*, 2010].

[59] The Mauna Loa observatory provides additional corroborative evidence that the stratospheric AOD was perturbed by the Sarychev eruption. While there are some differences between the derived lidar and AERONET AODs, both suggest perturbations that are readily detectable. Furthermore, the agreement in terms of the AOD between the modeling and the lidar is encouraging. Analysis of the wavelength-dependent perturbation to the AOD suggests that while there are still some significant uncertainties, the model size distribution for the optically active accumulation mode aerosol appears reasonable.

[60] *Hansen et al.* [2010] indicate that during June–July–August 2009, there was strong cooling over many continental regions of the Northern Hemisphere with North America being subject to cool anomalies in excess of −1 K. Our results suggest that, while the Sarychev eruption should act to cool Northern Hemisphere continents, the eruption of Sarychev cannot explain a cooling of this magnitude and is unlikely to be unambiguously detectable above the considerable climate variability. The favorable comparison of the SO$_2$ from the model with observations and the reasonable *e*-folding time for removal from the atmosphere suggests that should future eruptions of greater magnitude occur, these aspects at least should be relatively well modeled. Further work appears necessary to incorporate aerosol nucleation in the stratosphere so that the observed "lag" between the removal of SO$_2$ and the creation of optically active accumulation mode aerosol can be accurately modeled. Development of a dedicated stratospheric aerosol model would seem appropriate in this regard.

[61] The suggestion that deliberate stratospheric injection of SO$_2$ could be considered as a drastic measure to deal with a planetary emergency some time in the future should mitigation not be enough to deal with global warming has been studied [e.g., *Robock et al.*, 2008; *Rasch et al.*, 2008; *Jones et al.*, 2010a]. The favorable comparison of the SO$_2$ and sulfate (albeit with the "lag" mentioned above) from the model with observations puts the simulation of potential

geoengineering schemes on a firmer footing. The majority of geoengineering schemes [e.g., *Robock et al.*, 2008; *Jones et al.*, 2010a] have studied injection of SO$_2$ at tropical latitudes where the aerosol can be dispersed poleward in the meridional circulation associated with the westerly phase of the QBO [e.g., *Stenchikov et al.*, 2004]. However, *Jones et al.*, [2010b] show that this does little to ameliorate either the high-latitude warming in Arctic regions or the reduction of sea ice that are typical of future global warming scenarios. Our results tentatively show that injection of SO$_2$ into the stratosphere at higher latitudes could theoretically offset the high-latitude warming, but the effectiveness of injection would be significantly reduced owing to the much shorter lifetime of aerosols when compared to tropical injections (*e*-folding time for removal ~70–80 days rather than 12–14 months) and the lack of solar insolation at high latitudes. This modeling and observational evidence confirms the theoretical work of *Robock et al.* [2008] who suggest an *e*-folding time of around 3 months for removal of sulfate for Arctic injections and 12 months for tropical injections.

[62] While HadGEM2 may provide reasonable simulations of the transport and oxidation of SO$_2$ to sulfate aerosol, there are still some particular aspects that require refining, in particular the lack of representation of nucleation means that the transformation of SO$_2$ to optically active accumulation mode sulfate appears too quick when compared to observations. The observational data from OSIRIS has proved an extremely useful constraint for the model. A strong concern is that since the loss of SAGE III we are extremely reliant on OSIRIS which was launched on the ODIN satellite in 2001 with a lifetime requirement of just 2 years. That high-quality data are still available is extremely fortuitous.

References

Ammann, C. A., G. A. Meehl, and W. Washington (2003), A monthly and latitudinally varying volcanic forcing dataset in simulations of 20th century climate, *Geophys. Res. Lett.*, *30*(12), 1657, doi:10.1029/2003GL016875.

Baran, A. J., and J. S. Foot (1994), A new application of the operational sounder HIRS in determining a climatology of sulphuric acid aerosol from the Pinatubo eruption, *J. Geophys. Res.*, *99*, 25,673–25,679, doi:10.1029/94JD02044.

Barnes, J. E., and D. J. Hofmann (1997), Lidar measurements of stratospheric aerosol over Mauna Loa Observatory, *Geophys. Res. Lett.*, *24*, 1923–1926, doi:10.1029/97GL01943.

Bellouin, N., A. Jones, J. M. Haywood, and S. A. Christopher (2008a), Updated estimate of aerosol direct radiative forcing from satellite

observations and comparison against the Hadley Centre climate model, *J. Geophys. Res.*, 113, D10205, doi:10.1029/2007JD009385.

Bellouin, N., O. Boucher, J. M. Haywood, C. Johnson, A. Jones, J. Rae, and S. Woodward (2008b), Improved representation of aerosols for HadGEM2, *Tech. Note 73*, Met Office Hadley Centre, Exeter, U. K. (Available at http://www.metoffice.gov.uk/publications/HCTN/index.html.)

Bitar, L., T. J. Duck, N. I. Kristiansen, A. Stohl, and S. Beauchamp (2010), Lidar observations of Kasatochi volcano aerosols in the troposphere and stratosphere, *J. Geophys. Res.*, 115, D00L13, doi:10.1029/2009JD013650.

Bluth, G. J. S., S. D. Doiron, C. C. Schnetzler, A. J. Krueger, and L. S. Walter (1992), Global tracking of the SO_2 clouds from the June 1991 Mount Pinatubo eruptions, *Geophys. Res. Lett.*, 19, 151–154, doi:10.1029/91GL02792.

Bluth, G. J. S., W. I. Rose, I. E. Sprod, and A. J. Krueger (1997), Stratospheric loading from explosive volcanic eruptions, *J. Geol.*, 105, 671–684, doi:10.1086/515972.

Bourassa, A. E., D. A. Degenstein, R. L. Gattinger, and E. J. Llewellyn (2007), Stratospheric aerosol retrieval with OSIRIS limb scatter measurements, *J. Geophys. Res.*, 112, D10217, doi:10.1029/2006JD008079.

Bourassa, A. E., D. A. Degenstein, and E. J. Llewellyn (2008), Retrieval of stratospheric aerosol size information from the OSIRIS limb scattered sunlight spectra, *Atmos. Chem. Phys.*, 8, 6375–6380, doi:10.5194/acp-8-6375-2008.

Bourassa, A. E., D. A. Degenstein, B. J. Elash, and E. J. Llewellyn (2010), Evolution of the stratospheric aerosol enhancement following the eruptions of Okmok and Kasatochi: Odin-OSIRIS measurements, *J. Geophys. Res.*, 115, D00L03, doi:10.1029/2009JD013274.

Carn, S. A., A. J. Prata, N. A. Kroktov, K. Yang, and A. J. Krueger (2009), Satellite measurements of volatile emissions from recent North Pacific Arc eruptions, paper presented at Geological Society of America Annual Meeting, Portland, Ore.

Carslaw, K. C., and B. Kärcher (2006), Stratospheric aerosol processes, in *Assessment of Stratospheric Aerosol Properties*, edited by L. Thomason and T. Peter, *WCRP 124, WMO/TD 1295, SPARC Rep. 4*, World Meteorol. Organ., Geneva, Switzerland.

Clarisse, L., P.-F. Coheur, A. J. Prata, D. Hurtmans, A. Razavi, T. Phulpin, J. Hadji-Lazaro, and C. Clerbaux (2008), Tracking and quantifying volcanic SO_2 with IASI, the September 2007 eruption at Jebel at Tair, *Atmos. Chem. Phys.*, 8, 7723–7734, doi:10.5194/acp-8-7723-2008.

Clarisse, L., D. Hurtmans, A. J. Prata, F. Karagulian, C. Clerbaux, M. De Mazière, and P.-F. Coheur (2010), Retrieving radius, concentration, optical depth and mass of different types of aerosols from high resolution infrared nadir spectra, *Appl. Opt.*, 49, 3713–3722.

Clerbaux, C., et al. (2009), Monitoring of atmospheric composition using the thermal infrared IASI/MetOp sounder, *Atmos. Chem. Phys.*, 9, 6041–6054, doi:10.5194/acp-9-6041-2009.

Collins, W. J., et al. (2008), Evaluation of the HadGEM2 model, *Tech. Note 74*, Met Office Hadley Centre, Exeter, U. K. (Available at http://www.metoffice.gov.uk/publications/HCTN/index.html.)

d'Almeida, G. A., P. Koepke, and E. Shettle (1991), *Atmospheric Aerosols: Global Climatology and Radiative Characteristics*, A. Deepak, Hampton, Va.

d'Amico, G., et al. (2010), Stratospheric aerosol layers over southern Italy during the summer of 2009: Lidar observations and model comparison, paper presented at 25th International Laser Radar Conference, Int. Radiat. Comm., Int. Assoc. of Meteorol. and Atmos. Phys., St. Petersburg, Russia.

Deshler, T., and R. Anderson-Sprecher (2006), Non-volcanic stratospheric aerosol trends: 1971–2004, in *Assessment of Stratospheric Aerosol Properties*, edited by L. Thomason and T. Peter, *WCRP 124, WMO/TD 1295, SPARC Rep. 4*, World Meteorol. Organ., Geneva, Switzerland.

Deshler, T., M. E. Hervig, D. J. Hofmann, J. M. Rosen, and J. B. Liley (2003), Thirty years of in situ stratospheric aerosol size distribution measurements from Laramie, Wyoming (41°N), using balloon-borne instruments, *J. Geophys. Res.*, 108(D5), 4167, doi:10.1029/2002JD002514.

Dubovik, O., B. N. Holben, T. F. Eck, A. Smirnov, Y. J. Kaufman, M. D. King, D. Tanré, and I. Slutsker (2002), Variability of absorption and optical properties of key aerosol types observed in worldwide locations, *J. Atmos. Sci.*, 59, 590–608, doi:10.1175/1520-0469(2002)059<0590:VOAAOP>2.0.CO;2.

Echle, G., T. von Clarmann, and H. Oelhaf (1998), Optical and microphysical parameters of the Mt. Pinatubo aerosol as determined from MIPAS-B mid-IR limb emission spectra, *J. Geophys. Res.*, 103, 19,193–19,211, doi:10.1029/98JD01363.

Hansen, J., R. Ruedy, M. Sato, and K. Lo (2010), Global surface temperature change, *Rev. Geophys.*, doi:10.1029/2010RG000345, in press.

Haywood, J. M., and K. P. Shine (1995), The effect of anthropogenic sulfate and soot aerosol on the clear sky planetary radiation budget, *Geophys. Res. Lett.*, 22, 603–606, doi:10.1029/95GL00075.

Haywood, J. M., and K. P. Shine (1997), Multi-spectral calculations of the direct radiative forcing of tropospheric sulphate and soot aerosols using a column model, *Q. J. R. Meteorol. Soc.*, 123, 1907–1930, doi:10.1002/qj.49712354307.

Haywood, J. M., D. L. Roberts, A. Slingo, J. M. Edwards, and K. P. Shine (1997), General circulation model calculations of the direct radiative forcing by anthropogenic sulphate and fossil-fuel soot aerosol, *J. Clim.*, 10, 1562–1577, doi:10.1175/1520-0442(1997)010<1562:GCMCOT>2.0.CO;2.

Hoffmann, A., C. Ritter, M. Stock, M. Maturilli, and R. Neuber (2010), Lidar measurements of the Kasatochi aerosol plume in August and September 2008 in Ny-Ålesund, Spitsbergen, *J. Geophys. Res.*, 115, D00L12, doi:10.1029/2009JD013039.

Hofmann, D., J. Barnes, M. O'Neill, M. Trudeau, and R. Neely (2009), Increase in background stratospheric aerosol observed with lidar at Mauna Loa Observatory and Boulder, Colorado, *Geophys. Res. Lett.*, 36, L15808, doi:10.1029/2009GL039008.

Holben, B. N., et al. (1998), AERONET: A federated instrument network and data archive for aerosol characterization, *Remote Sens. Environ.*, 66, 1–16, doi:10.1016/S0034-4257(98)00031-5.

Jäger, H., and T. Deshler (2002), Lidar backscatter to extinction, mass and area conversions for stratospheric aerosols based on midlatitude balloonborne size distribution measurements, *Geophys. Res. Lett.*, 29(19), 1929, doi:10.1029/2002GL015609.

Jäger, H., and T. Deshler (2003), Correction to "Lidar backscatter to extinction, mass and area conversions for stratospheric aerosols based on midlatitude balloonborne size distribution measurements", *Geophys. Res. Lett.*, 30(7), 1382, doi:10.1029/2003GL017189.

Johnson, C. E., G. W. Mann, N. Bellouin, F. M. O'Connor, and M. Dalvi (2010), Comparison between UKCA-MODE and CLASSIC aerosol schemes in HadGEM3, *CR-ICP-2007-2012, Prod. 3.2*, Met Office Hadley Centre, Exeter, U. K.

Jones, A., D. L. Roberts, M. J. Woodage, and C. E. Johnson (2001), Indirect sulphate aerosol forcing in a climate model with an interactive sulphur cycle, *J. Geophys. Res.*, 106, 20,293–20,310, doi:10.1029/2000JD000089.

Jones, A., J. M. Haywood, O. Boucher, B. Kravitz, and A. Robock (2010a), Geoengineering by stratospheric SO_2 injection: Results from the Met Office HadGEM2 climate model and comparison with the Goddard Institute for Space Studies ModelE, *Atmos. Chem. Phys.*, 10, 5999–6006, doi:10.5194/acp-10-5999-201010.

Jones, A., J. M. Haywood, and O. Boucher (2010b), A comparison of the climate impacts of geoengineering by stratospheric SO_2 injection and by brightening of marine stratocumulus cloud, *Atmos. Sci. Lett.*, doi:10.1002/asl.291.DOI:10.1002/asl.291, in press.

Karagulian, F., L. Clarisse, C. Clerbaux, F. Prata, D. Hurtmans, and P.-F. Coheur (2010), Detection of volcanic SO_2, ash and H_2SO_4 using the Infrared Atmospheric Sounding Interferometer (IASI), *J. Geophys. Res.*, 115, D00L02, doi:10.1029/2009JD012786.

Kravitz, B., A. Robock, and A. Bourassa (2010), Negligible climatic effects from the 2008 Okmok and Kasatochi volcanic eruptions, *J. Geophys. Res.*, 115, D00L05, doi:10.1029/2009JD013525.

Krotkov, N. A., S. A. Carn, A. J. Krueger, P. K. Bhartia, and K. Yang (2006), Band residual difference algorithm for retrieval of SO_2 from the Aura Ozone Monitoring Instrument (OMI), *IEEE Trans. Geosci. Remote Sens.*, 44(5), 1259–1266, doi:10.1109/TGRS.2005.861932.

Lamb, H. H. (1970), Volcanic dust in the atmosphere, with a chronology and assessment of its meteorological significance, *Philos. Trans. R. Soc. London A*, 266, 425–533, doi:10.1098/rsta.1970.0010.

Llewellyn, E. J., et al. (2004), The OSIRIS instrument on the Odin spacecraft, *Can. J. Phys.*, 82, 411–422.

Martinsson, B. G., C. A. M. Brenninkmeijer, S. A. Carn, M. Hermann, K.-P. Heue, P. F. J. van Velthoven, and A. Zahn (2009), Influence of the 2008 Kasatochi volcanic eruption on sulfurous and carbonaceous aerosol constituents in the lower stratosphere, *Geophys. Res. Lett.*, 36, L12813, doi:10.1029/2009GL038735.

Newhall, C. G., and S. Self (1982), The Volcanic Explosivity Index (VEI): An estimate of explosive magnitude for historical volcanism, *J. Geophys. Res.*, 87, 1231–1238, doi:10.1029/JC087iC02p01231.

Oman, L., A. Robock, G. Stenchikov, G. A. Schmidt, and R. Ruedy (2005), Climatic response to high-latitude volcanic eruptions, *J. Geophys. Res.*, 110, D13103, doi:10.1029/2004JD005487.

Prata, A. J., S. A. Carn, A. Stohl, and J. Kerkmann (2007), Long range transport and fate of a stratospheric volcanic cloud from Soufrière Hills volcano, Montserrat, *Atmos. Chem. Phys.*, 7, 5093–5103, doi:10.5194/acp-7-5093-2007.

Prata, A. J., G. Gangale, L. Clarisse, and F. Karagulian (2010), Ash and sulphur dioxide in the 2008 eruptions of Okmok and Kasatochi: Insights

from high spectral resolution satellite measurements, *J. Geophys. Res.*, doi:10.1029/2009JD013556, in press.

Rasch, P. J., S. Tilmes, R. P. Turco, A. Robock, L. Oman, C.-C. Chen, G. L. Stenchikov, and R. R. Garcia (2008), An overview of geoengineering of climate using stratospheric sulphate aerosols, *Philos. Trans. R. Soc. A*, *366*, 4007–4037, doi:10.1098/rsta.2008.0131.

Rix, M., et al. (2009), Satellite monitoring of volcanic sulfur dioxide emissions for early warning of volcanic hazards, *IEEE J. Selec. Top. Appl. Earth Obs. Remote Sens.*, *2*(3), 196–206, doi:10.1109/JSTARS.2009.2031120(JSTARS).

Robock, A. (2000), Volcanoes and climate, *Rev. Geophys.*, *38*(2), 191–219, doi:10.1029/1998RG000054.

Robock, A., L. Oman, and G. L. Stenchikov (2008), Regional climate responses to geoengineering with tropical and Arctic SO_2 injection, *J. Geophys. Res.*, *113*, D16101, doi:10.1029/2008JD010050.

Russell, P. B., et al. (1993), Pinatubo and pre-Pinatubo optical-depth spectra: Mauna Loa measurements, comparisons, inferred particle size distributions, radiative effects, and relationship to lidar data, *J. Geophys. Res.*, *98*, 22,969–22,985, doi:10.1029/93JD02308.

Sato, M., J. E. Hansen, M. P. McCormick, and J. B. Pollack (1993), Stratospheric aerosol optical depths, 1850–1990, *J. Geophys. Res.*, *98*, 22,987–22,994, doi:10.1029/93JD02553.

Schulz, M., et al. (2006), Radiative forcing by aerosols as derived from the AeroCom present-day and pre-industrial simulations, *Atmos. Chem. Phys.*, *6*, 5225–5246, doi:10.5194/acp-6-5225-2006.

Staniforth, A., and J. Côté (1991), Semi-Lagrangian integration schemes for atmospheric models—A review, *Mon. Weather Rev.*, *119*(9), 2206–2223, doi:10.1175/1520-0493(1991)119<2206:SLISFA>2.0.CO;2.

Stenchikov, G., K. Hamilton, A. Robock, V. Ramaswamy, and M. D. Schwarzkopf (2004), Arctic oscillation response to the 1991 Pinatubo eruption in the SKYHI general circulation model with a realistic quasi-biennial oscillation, *J. Geophys. Res.*, *109*, D03112, doi:10.1029/2003JD003699.

Stothers, R. B. (1997), Stratospheric aerosol clouds due to very large volcanic eruptions of the early twentieth century: Effective particle sizes and conversion from pyrheliometric to visual optical depth, *J. Geophys. Res.*, *101*, 19,245–19,250.

Stothers, R. B. (2001), A chronology of annual mean effective radii of stratospheric aerosols from volcanic eruptions during the twentieth century as derived from ground-based spectral extinction measurements, *J. Geophys. Res.*, *106*, 32,043–32,049, doi:10.1029/2001JD000414.

Telford, P., P. Braesicke, O. Morgenstern, and J. Pyle (2008), Technical note: Description and assessment of a nudged version of the new dynamics Unified Model, *Atmos. Chem. Phys.*, *8*, 1,701–1,712.

Telford, P., P. Braesicke, O. Morgenstern, and J. Pyle (2009), Reassessment of causes of ozone column variability following the eruption of Mount Pinatubo using a nudged CCM, *Atmos. Chem. Phys.*, *9*, 4251–4260, doi:10.5194/acp-9-4251-2009.

Thomason, L. W., M. C. Pitts, and D. M. Winker (2007), CALIPSO observations of stratospheric aerosols: A preliminary assessment, *Atmos. Chem. Phys.*, *7*, 5283–5290, doi:10.5194/acp-7-5283-2007.

Winker, D. M., W. H. Hunt, and M. J. McGill (2007), Initial performance assessment of CALIOP, *Geophys. Res. Lett.*, *34*, L19803, doi:10.1029/2007GL030135.

Yang, K., N. A. Krotkov, A. J. Krueger, S. A. Carn, P. K. Bhartia, and P. F. Levelt (2007), Retrieval of large volcanic SO_2 columns from the Aura Ozone Monitoring Instrument (OMI): Comparison and limitations, *J. Geophys. Res.*, *112*, D24S43, doi:10.1029/2007JD008825.

P. Agnew, Forecasting Research and Development, Met Office, FitzRoy Road, Exeter EX1 3PB, UK.

J. Barnes, Mauna Loa Observatory, NOAA, c/o NCAR High Altitude Observatory, PO Box 3000, Boulder, CO 80307-3000, USA.

N. Bellouin, O. Boucher, J. M. Haywood, and A. Jones, Met Office Hadley Centre, FitzRoy Road, Exeter EX1 3PB, UK. (jim.haywood@metoffice.gov.uk)

A. Bourassa and D. Degenstein, ISAS, University of Saskatchewan, 116 Science Pl., Saskatoon, SK S7N5E2, Canada.

P. Braesicke and P. Telford, NCAS Climate, Centre for Atmospheric Science, University of Cambridge, Cambridge CB2 1EW, UK.

L. Clarisse and P. Coheur, Spectroscopie de l'Atmosphère, Service de Chimie Quantique et Photophysique, Université Libre de Bruxelles, B-1050 Brussels, Belgium.

C. Clerbaux, UPMC Université Paris 06, Université Versailles St.-Quentin, CNRS/INSU, LATMOS-IPSL, F-75005 Paris, France.